An automated feeding system for the African killifish reveals effects of dietary restriction on lifespan and allows scalable assessment of associative learning

Andrew McKay[1,2,10], Emma K. Costa[3,4,10], Jingxun Chen[1,10], Chi-Kuo Hu[1], Xiaoshan Chen[1], Claire N. Bedbrook[1,5], Rishad C. Khondker[1], Mike Thielvoldt[6], Param Priya Singh[1], Tony Wyss-Coray[3,7,8], Anne Brunet[1,7,8,9]

[1]Department of Genetics, Stanford University, Stanford, CA 94305

[2]Biology Graduate Program, Stanford University, Stanford, CA 94305

[3]Department of Neurology and Neurological Sciences, Stanford University, Stanford, CA 94305

[4]Neurosciences Interdepartmental Program, Stanford University School of Medicine, Stanford, CA 94305

[5]Department of Bioengineering, Stanford University, Stanford, CA, USA 94305

[6]Thielvoldt Engineering, Albany, CA 94706

[7]Glenn Laboratories for the Biology of Aging, Stanford University, CA 94305

[8]Wu Tsai Neurosciences Institute, Stanford University, CA 94305

[9]Corresponding author: abrunet1@stanford.edu

[10]Equal contribution

Abstract

The African turquoise killifish is an exciting new vertebrate model for aging studies. A significant challenge for any model organism is the control over its diet in space and time. To address this

challenge, we created an automated and networked fish feeding system. Our automated feeder is designed to be open-source, easily transferable, and built from widely available components. Compared to manual feeding, our automated system is highly precise and flexible. As a proof-of-concept for the feeding flexibility of these automated feeders, we define a favorable regimen for growth and fertility for the African killifish and a dietary restriction regimen where both feeding time and quantity are reduced. We show that this dietary restriction regimen extends lifespan in males (but not in females) and impacts the transcriptomes of killifish livers in a sex-specific manner. Moreover, combining our automated feeding system with a video camera, we establish a quantitative associative learning assay to provide an integrative measure of cognitive performance for the killifish. The ability to precisely control food delivery in the killifish opens new areas to assess lifespan and cognitive behavior dynamics and to screen for dietary interventions and drugs in a scalable manner previously impossible with traditional vertebrate model organisms.

Introduction

The African turquoise killifish, *Nothobranchius furzeri*, is a new genetically tractable model organism that has been developed for the study of aging and "suspended animation" (embryonic diapause) (Cellerino et al., 2016; Harel and Brunet, 2015; Hu and Brunet, 2018; Platzer and Englert, 2016; Poeschla and Valenzano, 2020). This fish has a naturally compressed lifespan of 4-6 months, which is 6 times shorter than the maximum lifespan of mice and 10 times shorter than zebrafish (Harel and Brunet, 2015). In its short life, the African killifish exhibit hallmarks of aging, including cognitive decline (Valenzano et al., 2006a; Valenzano et al., 2006b), neurodegeneration

(Bagnoli et al., 2022; Matsui et al., 2019; Terzibasi et al., 2008), fertility decline (Api et al., 2018; Zak and Reichard, 2021), cellular senescence (Valenzano et al., 2006a), impaired regeneration and wound healing (Wendler et al., 2015), defects in heart function (Ahuja et al., 2019), and an increased risk of cancer (Baumgart et al., 2015; Di Cicco et al., 2011). A genetic and genomic toolkit has been developed for the killifish, including sequencing of its genome (Reichwald et al., 2015; Valenzano et al., 2015), Tol2-based transgenesis (Hartmann and Englert, 2012; Valenzano et al., 2011), and CRISPR/Cas9-mediated genome-editing (Harel et al., 2015). These developments have allowed disease modeling in the killifish (Harel et al., 2015), identification of genes potentially involved in lifespan differences (Reichwald et al., 2015; Valenzano et al., 2015) and sex determination (Reichwald et al., 2015; Valenzano et al., 2009), determination of enhancers involved in tissue regeneration (Wang et al., 2020), and discovery of chromatin regulators important for embryonic diapause (Hu et al., 2020).

A major challenge for any model system is the precise control of its diet. A proper diet is important for robust growth and fertility in colony maintenance and genetic manipulations. A controlled feeding regimen is also critical for lifespan studies, given the impact of dietary restriction – and more generally diet – on lifespan in a wide variety of species (Fontana and Partridge, 2015; Green et al., 2022; Longo and Anderson, 2022; Mair and Dillin, 2008), including worms (Houthoofd and Vanfleteren, 2007), flies (Partridge et al., 2005), killifish (Terzibasi et al., 2009), stickleback fish (Inness and Metcalfe, 2008), mice (Bartke et al., 2001; Mitchell et al., 2019; Weindruch et al., 1986), rats (Goodrick et al., 1983; Swindell, 2012; Turturro et al., 1999), and monkeys (Colman et al., 2009; Colman et al., 2014; Mattison et al., 2017; Mattison et al., 2012). Importantly, food is

not only essential for growth, fertility, and survival, but it can also serve as a reward. Indeed, several cognitive tests rely on the ability of associating food with a task (Flagel and Robinson, 2017; Jarrard, 1993; Meyer et al., 2012; Olton and Samuelson, 1976; Rudy and Sutherland, 1989).

In the wild, adult African turquoise killifish primarily feed upon small crustaceans and insect larvae ("bloodworms") that are present in their ephemeral ponds in Africa (Polacik and Reichard, 2010; Reichard and Polacik, 2019). In laboratory settings, African killifish are often fed using bloodworms, either live (Hartmann et al., 2011; Reichwald et al., 2015; Terzibasi et al., 2009; Wendler et al., 2015), frozen (Genade et al., 2005; Terzibasi et al., 2008; Valenzano et al., 2006b; Zupkovitz et al., 2018), or lyophilized (Harel et al., 2015; Hu et al., 2020; Valenzano et al., 2015). However, feeding with live bloodworms can introduce pathogens in the colony (Broza and Halpern, 2001; Moore et al., 2003; Rouf and Rigney, 1993), and the nutrition values of live bloodworms can vary depending on the lot and supplier (Fard et al., 2014). To alleviate these issues, dry food pellets have been recently adopted for killifish, either alone (Zak et al., 2020; Zak et al., 2022) or in combination with live food (Matsui et al., 2019). But a main challenge of dry fish food – and fish food in general – is that it needs to be delivered for each feeding, otherwise it loses its appeal to fish and remains uneaten in the tanks. Regardless of the type of food used in the laboratory, feeding fish is largely based on manual feeding. Hence, food delivery is a limiting factor: it is hard to perform in a consistent manner, to scale up, and to schedule at any time of the day or night. These features hamper the testing of different feeding regimens and other interventions. Control over food delivery will help the development of the killifish as a scalable model for lifespan and other traits and to allow interventions.

To address these challenges and develop the scalability of the killifish as a model system, we have created an automated feeding system for killifish feeding. We provide evidence that this system is precise and reliable, and that it allows controlled and tunable feeding throughout the day or night. Using this new flexible feeding system, we explore the parameters of diet in the killifish and identify a dietary restriction regimen that extends the lifespan of killifish and modulates liver transcriptome in a sex-specific manner. Interestingly, our automated feeders also allow us to design a novel associative learning assay to test cognitive function in the African killifish. This automated feeding system will help the development of the killifish as a high-throughput model for lifespan and will allow scalable intervention or drug screening.

Results

A wireless networked automated feeding system

Controlling feeding automatically is a critical component for the development and scalability of a model organism. Automated feeders have been developed for fish, but they are rarely used due to their imprecision (e.g., hobbyist feeding systems) or prohibitive costs (e.g., scientific-grade feeding systems, such as Tritone from Tecniplast). While systems developed for zebrafish have solved some of these constraints (Doyle et al., 2017; Lange et al., 2021), they are either not scalable to hundreds of animals simultaneously being fed or cannot easily be added onto commercial water systems. Thus, there is still a need for high precision and programmable feeders compatible with commonly used water systems.

To address the main limitations with current feeding methods, we developed a wireless networked automated feeding system for the African turquoise killifish. We created a system in which different components function independently to confer robustness and avoid single points of failure that affect the overall feeding scheme. This is particularly important when feeding needs to happen over a lifespan. The automated feeder that we designed and built is placed on top of each animal's 2.8 L tank (Figure 1A) and drops dry food (e.g., Otohime fish diet) from a small feed hopper (Figure 1B) directly into the tank (which houses one individual fish). The feeder is powered by an attached battery, and the food pellets are automatically segregated from the hopper by a rotating acrylic disc, with the resulting pieces of food dropping onto the water through a 3-mm diameter opening cut out in the supporting acrylic plate below (Figure 1C, Figure 1-figure supplement 1A, Figure 1-video 1). The 3-mm opening rotates from under the feed hopper, collects food, and travels to the drop site above the tank opening. Each rotation delivers a fixed volume of food, averaging around 5 mg in mass, and multiples of 5 mg can be programmed to increase food amount per feeding. Feedings are also fully programmable to any frequency or time of day by the user, and each feeder operates independently of one another (Figure 1-figure supplement 1B), allowing flexibility in feeding schedule (Table 1).

To determine whether food has indeed dropped into the tank, we designed the acrylic disc's opening such that it pushes the food between a photoresistor and a light-emitting diode (LED) before reaching the drop site. The photoresistor and LED provide confirmation for feeding by measuring the resistance of the photoresistor when food obstructs the light from the LED (outgoing

trip), and after feeding, when the empty food-receptacle 3-mm opening allows light to pass (return trip) (Figure 1-figure supplement 1A, steps 3-6). We also designed the feeder such that each feeder communicates feeding confirmations independently to a local server using the 802.11 wireless communication standard, which can then be aggregated across groups of feeders to a cloud-based server (Figure 1D). Thus, with our automated system, feedings can be recorded and backed up remotely, providing an automatic log for the user.

Lastly, the wireless communication and battery-powered function allows our system to function remotely and flexibly. This is an improvement over other automated systems (such as Tritone from Tecniplast), whose monolithic design creates many single points of system-wide failure, or over designs that are not networked or restricted to less flexible wire-based communication (Doyle et al., 2017; Manabe et al., 2013; Yang et al., 2019). We found that more than 100 automated feeders can operate simultaneously on the same local server. Additionally, our automated feeders are estimated to cost 12.88 USD per feeder (Figure 1-Source Data 1), so ~2,000 USD for >100 tanks (including network setup and operation cost for 2 years), which is significantly less expensive than commercial systems (for example, the Tecniplast Tritone system costs ~200,000 USD to feed approximately 240 tanks). Hence, our design for an automated feeding system allows controlled, tunable, and recorded feedings throughout the lifespan of the killifish.

Fidelity and precision of the automated feeding system

We tested the fidelity and precision of the automated feeding system. A representative feeder was set to deliver 7 feedings a day for 30 days, and food delivery was recorded on the server (Figure

1-figure supplement 1A, steps 3-6). Food delivery occurred 98.1% of the time (206 actual food delivery for 210 scheduled food deliveries; Figure 2A). Overall, aggregating 41 feeders for 2279 cumulative days showed that most food deliveries were fully accounted for (Figure 2B), with only 7.89% of days deviating by one unconfirmed food delivery (Figure 2C). This fidelity was confirmed independently with a separate set of automated feeders of the same design built independently by another researcher (Figure 2-figure supplement 1A, B).

We compared the precision of the mass of food dropped per delivery for our automated feeder versus manual feeding by individual users. Single or multiple automated feeders were more precise, by an order of magnitude, at delivering a given amount of food compared to a group of 6 different individuals (similar to what can be done in fish rooms to offset the workload) or a single individual measuring and delivering food (Figure 2D).

Because of its flexibility, the automated feeder can deliver up to 5 mg per unit every 10 minutes, or 720 mg per 12-hour period, representing a potential 20x increase over the baseline dietary regime for the day (Table 1). The automated feeder can also feed during the night if desired, which would not be practical for manual feeding. Thus, our automatic system decreases the amount of labor and provides high precision, reproducibility, and flexibility for husbandry and for varying diet regimens (Table 1).

Defining a daily dietary restriction feeding schedule in the killifish

We used our automated feeding system to define a variety of dietary regimens in killifish – dietary restriction and overfeeding. Dietary restriction has been shown to delay signs of aging and age-related diseases in multiple species (Fontana and Partridge, 2015; Green et al., 2022; Longo and Anderson, 2022; Mair and Dillin, 2008). Dietary restriction regimens encompass restricting overall food (Colman et al., 2009; Colman et al., 2014; Mattison et al., 2017; Mattison et al., 2012; Weindruch et al., 1986) or restricting the time of feeding during the day (Mitchell et al., 2019) or over longer periods (Brandhorst et al., 2015). In killifish, dietary restriction has been done by every other day feeding because it is difficult to do otherwise with manual feeding (Terzibasi et al., 2009). A dietary restriction regimen is expected to reduce growth and fertility (especially when applied early in adulthood) compared to an *ad libitum* feeding regimen. In contrast, overfeeding has negative consequences on health, and it is expected to increase growth but to reduce fertility compared to an *ad libitum* regimen (Magwere et al., 2004). To define different dietary regimens in the African turquoise killifish, we fed individually housed male and female killifish – starting in young adults (1 month of age) – and varied both the amount and timing of feedings throughout the day using our programmable automated feeders. For "*ad libitum*" (AL, blue), we fed 35 mg of dry food per day, in 7 feedings of 5 mg evenly spaced over 12 hours of the day, for a total of 245 mg per week (roughly similar to manual feeding) (Figure 3A). For "dietary restriction" (DR, orange), we fed 15 mg per day (~57% restriction), in 3 feedings of 5 mg over 2 hours, for a total of 105 mg per week (Figure 3A). This DR regimen is both amount- and time-restricted (achieving amount-restriction without time restriction would not be possible in current settings because of the minimum 5 mg delivery amount of automated feeder, see above). This DR regimen led to smaller (Figure 3B and C) and less fertile (Figure 3D, Figure 3-figure supplement 1A, B) animals than the

AL regimen, consistent with what is expected under dietary restriction. Importantly, at 7 feedings of 5 mg a day (AL), animals were not overfed because they could be fed more (12 feedings of 5 mg a day) (Figure 3E), and this extra-feeding increased size (Figure 3F and G) but decreased fertility (Figure 3H, Figure 3-figure supplement 1C, D). Hence, a favorable feeding regimen, at least under these husbandry conditions, is around 7 feedings per day and 35 mg of food per day for the African killifish. Together, these experiments define diets that optimize growth and fertility in the African killifish (for these husbandry conditions), and they identify a dietary restriction regimen in this species.

An amount- and time-restricted diet regimen extends lifespan in a sex-specific manner

We asked if the amount- and time-restricted DR regimen defined above could promote longevity in the killifish. To this end, we assessed the lifespan of female and male African killifish in *ad libitum* (AL, blue: 7 evenly spaced feedings of 5 mg per day over 12 hours of the day) or the amount- and time-restricted conditions (DR, orange: amount- and time-restricted: 3 feedings of 5 mg per day over 2 hours in the morning) (Figure 4A). We enrolled young adult animals in two independent cohorts (33 males and 26 females in cohort 1 (Figure 4-figure supplement 1A), and 43 males and 49 females in cohort 2 (Figure 4A)). The DR regimen was initiated in young adults (1 month of age) and lasted until death (Figure 4A). Interestingly, males fed the DR diet (orange) lived longer than those fed the AL diet (blue; 16.6% median lifespan extension for cohort 1 (Figure 4-figure supplement 1B), 22.1% median lifespan extension for cohort 2 (Figure 4B)). In contrast, females fed the DR diet did not live significantly longer than those fed the AL diet in either cohort (Figure 4C, Figure 4-figure supplement 1C). Animals fed a DR diet exhibited lifespan differences

between sexes, with male living significantly longer than females (Figure 4D and E, Figure 4-figure supplement 1D and E). The sex-specific effect of DR on killifish lifespan was also supported using Cox Proportional Hazards in a factorial design (Figure 4-Source data 3), where the interaction term between sex and dietary regimen was found to be significant ($p = 0.045$). Furthermore, fitting the survival data of male killifish into a Gompertz distribution resulted in an estimated reduced slope for males in DR conditions. These results suggest that this DR regimen reduces the "rate of aging" in male killifish (Figure 4F), in line with the effect of intermittent feeding on lifespan (Terzibasi et al., 2009). Thus, this DR regimen (restricted in time and amount) significantly extends the lifespan of males, but not females, in the African killifish.

An amount- and time-restricted diet regimen impacts the liver transcriptome in a sex-specific manner

To determine whether this amount- and time-restricted DR regimen could impact gene expression in a sex-specific manner, we generated transcriptomic datasets. We focused on liver and brain because of their known roles in systemic metabolism and dietary response (Ye and Medzhitov, 2019). Using the automated feeders, we initiated DR or AL regimens in females and males at the young adult stage (1 month of age) and fed them these regimens for 5 weeks (Figure 5A). We then collected livers and brains for RNA-sequencing (RNA-seq) (Figure 5A). Principal component analysis (PCA) on the full transcriptomes showed strong separation by sex in the liver in the AL condition, and this separation was even larger in the DR condition (Figure 5B, Figure 5-figure supplement 1A). In contrast, PCA did not reveal detectable separation by sex or diet in the brain

(Figure 5B, Figure 5-figure supplement 1B). Thus, liver gene expression is sex specific in AL and DR conditions, and this sexual dimorphism is exacerbated in the DR condition.

We next identified the set of genes that are differentially regulated by diet (AL vs DR) for each sex. This analysis yielded 221 differential expressed genes between AL and DR conditions ("diet DEGs") for females and 70 diet DEGs for males ($p < 0.05$), with 10 genes shared between the two sexes (Figure 5-figure supplement 1C). Gene Set Enrichment Analysis (GSEA) revealed that fatty acid and acetyl-CoA metabolism genes (e.g., *FADS2*, *ACSS2*, *DGAT2*, *SCD5*) were strongly downregulated in the liver in response to DR in females, but less so in males (Figure 5C, D, Figure 5-Source Data 6, 7). Protein folding and ER stress response pathways (e.g., *HSP90B1*, *DNAJB11*, *SDF2L1*, *DERL1*) were strikingly upregulated in the liver in response to DR in females, but not in males (Figure 5C, D). Hypergeometric Gene Ontology (GO) enrichment analysis of the diet DEGs confirmed both observations (see Materials and Methods, Figure 5-figure supplement 1D, Figure 5-Source Data 8). Finally, GSEA (but not the hypergeometric GO analysis) showed that genes involved in inflammation-related pathways – positive regulators of immune responses, leukocyte activation, and cytokine-mediated signaling (e.g., *CMKLR1*, *TBK1*, *BCL6*) – were strongly downregulated in response to DR in the liver in males, but less so in females (Figure 5C, D). Thus, the sex-specific response to diet in the liver involves lipid metabolism, protein homeostasis, and inflammatory signaling pathways.

We also identified the set of genes that are differentially regulated by sex (male vs. females) for each regimen ("sex DEGs"). Interestingly, sex DEGs (in either AL or DR) were significantly

264 enriched in the diet DEGs of either males or females, controlling for gene expression distribution
265 and gene set size (Figure 5E, Figure 5-figure supplement 1E). These results indicate that DR
266 preferentially modulates sexually dimorphic genes in the liver, perhaps because of the different
267 metabolic needs of males and females for reproduction. Collectively, these observations indicate
268 that an amount- and time-restricted DR regimen impacts the expression of metabolic and
269 stress/inflammatory pathways in the liver in a sex-specific manner, and this may underlie the
270 beneficial effects of DR on male, but not female lifespan.
271
272 **Using automated feeders to develop a positive associative learning assay for the killifish**
273 Food not only influences growth, fertility, and lifespan, but it is also a potent reward across species,
274 including humans (Lutter and Nestler, 2009). The rewarding aspect of food has been used for
275 developing feeding-associated learning behaviors in many model organisms, including worms
276 (Cho et al., 2016; Kauffman et al., 2010; Lim et al., 2018; Stein and Murphy, 2014), flies (Das et
277 al., 2014), zebrafish (Doyle *et al.*, 2017; Pylatiuk et al., 2019; Sison and Gerlai, 2010), mice
278 (Steinberg et al., 2020), and non-human primates (Rolls, 2006). Assaying learning behavior over
279 an animal's lifetime provides a way of examining functional decline with age. An aversive learning
280 assay has been previously established in killifish and revealed age-dependent decline (Valenzano
281 et al., 2006a; Valenzano et al., 2006b). However, repetitive exposure to aversive stimuli may
282 induce stress responses that could affect lifespan. It would be helpful to develop a learning
283 behavior assay for killifish that would require little manipulation of an animal and would use an
284 appetitive stimulus rather than an aversive one to limit stress-related responses.
285

We used our programmable feeding platform to establish a positive associative behavior ("learning") assay, also known as classical conditioning or Pavlovian conditioning. For this assay, we used a red light above the tank as the "conditioned stimulus" and food delivered by the automated feeder as the "unconditioned stimulus". We integrated a red LED light into the automated feeding system, and we added an individual camera facing the front of each killifish's 2.8 L tank for video recording (Figure 6A). The red LED light turns on 2 seconds after video recording starts and 7 seconds later, the food is automatically dropped by the feeder to the water surface (Figure 6A).

We analyzed the video recordings of killifish (a total of 16 males and females, 47-130 days of age) using the automated tracking software DeepLabCut (Mathis et al., 2018) (Figure 6B). We tracked individual fish trajectories (Figure 6C, D). An association was defined as "successful" when a fish initiated a surface-bound trajectory after the red light turned on (2 seconds after the video recording started) but before the food dropped to the water surface (7 seconds after the light turned on, so 9 seconds after the recording started) (Figure 6C, bottom, Figure 6-video 1, see Materials and Methods). An association was defined as "unsuccessful" when a fish did not initiate a surface-bound trajectory within this window of time (Figure 6C, top, Figure 6-video 2). Qualitative comparisons of the trajectory traces of individual fish (Figure 6D) or Compass plots to display trajectory directionality of all fish (Figure 6-figure supplement 1A) both suggest that individual fish initiate a surface-bound trajectory more prominently in later trials than in earlier ones. To quantify this surface-bound trajectory, we established an automated pipeline (Figure 6B). We first calculated velocity (i.e., pixels traversed per second) for each fish and assessed the "bursts" of

velocity (yellow regions in Figure 6E) for each animal in each trial (see Materials and Methods). We then used this metric to plot, for each fish, the time of the first trajectory toward the water surface (t_1) to reflect "initiation of surface-bound trajectory" (Figure 6F). For stringent quantification, we only scored the videos of fish that ate during the assay (13 fish out of 16 total), because a successful eating behavior indicates that the fish could see the food at the surface and was motivated enough to move (see Materials and Methods). The average time of the first surface-bound trajectory for these 13 fish was significantly shorter in the last 7 trials than in the first 7 trials ($p = 0.0005$) (Figure 6G). The percentage of successful trials in the last 7 trials was also significantly higher than that in the first 7 trials ($p = 0.030$) (Figure 6H). These results were confirmed by manual quantification (Figure 6-figure supplement 1B-E), with a correlation of 0.80 for t_1 (Figure 6-figure supplement 1F). Thus, after several trials, killifish move toward the food delivery when the light turns on but before the food drops, consistent with a positive association between red light and food.

We next compared the association performance between young and old animals (grouping both sexes). We verified that the average velocity of young and old fish did not exhibit overt differences, suggesting that old fish could overall move (Figure 6-figure supplement 1G). Old animals ($n = 8$ males and females, 119-130 days of age) tended to have slightly poorer association performance compared to young ones ($n = 5$ males and females, 47-70 days of age) (Figure 6I-K). Old animals also tended to have a lower "Learning index"– defined as the inverse of the first trial number needed for an animal to achieve 2 consecutive successes (see Materials and Methods) (Figure 6L). However, at this sample size, the differences between ages were not statistically significant

whether animals were binned into young and old categories (Figure 6J-L) or not (regression, Figure 6M). To detect the observed effect size between young and old (Cohen's d = -0.786) at a P-value of 0.05 and power of 80%, we estimated that 28 animals per age group would be needed when using learning index (and 27 and 132 animals per age group when using average time of first surface-bound trajectory and percentage of success, respectively). Collectively, these results indicate that the automated feeders can be used to determine associative conditioning, a measure of cognitive fitness that could be adapted for future aging studies.

Discussion

The automated feeding system presented here provides a valuable resource to the killifish community to consistently and reproducibly control the critical factor of feeding. Our system also offers an increased resolution on diet's impact on lifespan in a vertebrate model of aging. The automated feeders improve the precision of food dropped compared to manual feeding, which could reduce variability in experiments (e.g., lifespan studies) and deliver a well-defined diet. Compared to feeding approaches that risk introducing infection (live food) or are labor intensive (manual feeding), our feeding system is a safe and modular solution to feeding not only killifish and other teleost model organisms such as medaka, stickleback, or zebrafish. Furthermore, the tunable frequency and quantity of feedings that can be programmed opens up an experimental space (e.g., night feeding) previously infeasible with conventional feeding approaches. Our design also allows each tank to have its own food hopper and allows straightforward nutrient and drug testing, such as high-fat diets, ketogenic diets (Newman et al., 2017; Roberts et al., 2017), or dosing of animals with drug-encapsulated food (Valenzano et al., 2006b). While there are still areas for

optimization, including improved battery life and a simplified user interface, the performance of our automated feeding system is beyond that of manual feeding or several other automated feeding systems (Doyle et al., 2017; Manabe et al., 2013; Yang et al., 2019) in terms of combining precise amount of food dropped, modularity, and scalability. Compared to other recently developed scalable designs (Lange et al., 2021), our automated feeders can be added to any tank, including tanks from commercial water systems, allowing flexibility in experimental design.

Using the automated feeding system, we explore dietary parameters and identify a feeding regimen close to an *ad libitum* diet, as well as a daily dietary restriction diet for the African killifish. We note that the median and maximum lifespan of the killifish in *ad libitum* conditions in the experiments presented in this study are shorter than some previous studies (Hu et al., 2020), though longer than others (Terzibasi et al., 2008; Valenzano et al., 2006b). These differences might be linked to food amount or supply differences or other husbandry differences, and "*ad libitum*" conditions may in fact vary depending on animal facilities. We also show that the amount- and time-restricted diet we used (~57% dietary restriction) extends the lifespan of male, but not female killifish. Gompertz analysis confirms that dietary restriction reduces the rate of aging in males only. This sex difference in lifespan extension is likely independent of killifish social dynamics, as all animals were housed individually. Lifespan differences between sexes in response to DR is also observed in other species (Bronikowski et al., 2022). In mice, extreme DR (40%) extends lifespan in males, but not in females (Mitchell et al., 2016), though milder DR leads to a greater lifespan extension in females than males (Bonkowski et al., 2006; Kane et al., 2018; Mitchell et al., 2016). Different strains of mice exhibit more lifespan extension in response to DR in males

374 than in females (Liao et al., 2010). In flies, DR has also been shown to impact lifespan differently
375 between the sexes, with female flies enjoying the maximum lifespan benefits from DR at higher
376 calorie levels than male flies (Magwere et al., 2004). In *C. elegans*, DR is more beneficial in
377 hermaphrodites than in males (Honjoh et al., 2017). Collectively, these observations suggest that
378 sexes respond differently to various DR regimens and that females may not tolerate extreme DR
379 regimens.
380
381 We also examine the gene expression changes associated with the sex-specific response to DR in
382 the African turquoise killifish. We find that amount- and time-restricted DR downregulates fatty
383 acid synthesis genes in the liver in females, more so than in males. In mice, DR also downregulates
384 lipid metabolic genes (e.g., *ACYL*, *AACS*) in females (Hahn et al., 2017), which has been proposed
385 to protect older animals from visceral fat accumulation (Kuhla et al., 2014) and hepatic insulin
386 resistance (Hahn et al., 2017). It is possible that in female killifish, the decrease in lipid enzyme
387 expression in the liver in response to the amount- and time-restricted DR regimen is too
388 pronounced and not compatible with sustained metabolic function. DR also upregulates protein
389 folding and ER stress response pathways in female but not male killifish. This was not observed
390 in female mice upon DR (Hahn et al., 2017), and this may reflect a response to extreme DR to
391 meet higher secretory demand or protein misfolding stress. Finally, DR downregulates
392 inflammation-related pathways in female killifish, but less prominently than in males. DR was also
393 able to reduce inflammation in female mice (Swindell, 2008; 2009), and this decreased
394 inflammation may contribute to delay the aging process in mammals (Hunt et al., 2019; Maeso-
395 Diaz et al., 2018; Swindell, 2009). But in killifish, the blunted ability of DR to reduce inflammation

396 in females compared to males may also contribute to the lack of lifespan extension by this DR
397 regimen in females. It is possible that the DR regimen defined here is too severe to provide lifespan
398 benefits to females, and AL and DR regimens would likely need to be optimized differently in
399 males and females.
400
401 Using the killifish feeding system, we establish a proof-of-concept, positive association learning
402 assay (classical conditioning) that couples food with a red LED light. Combining video cameras
403 with feeders allows many animals to be conditioned simultaneously, at any time, with the ability
404 to collect a wealth of information about animal behavior without investigator-induced disturbance.
405 A positive association learning assay is advantageous over a negative one because it is less stressful
406 for the animal and could be done in conjunction with a lifespan assay without inducing additional
407 perturbation. However, food amounts dispensed for the assay itself would need to be carefully
408 accounted for in the total amount, to avoid inadvertently affecting the overall diet and the lifespan
409 of the animal.
410
411 The current version of the positive association assay has limitations. First, it only uses one camera
412 for recording fish behavior, and three-dimensional (3D) behaviors are not fully captured. This
413 assay would therefore be enhanced by using other deep learning methods that better predict 3D
414 poses from monocular (2D) video footage (Dunn et al., 2021; Gosztolai et al., 2021; Karashchuk
415 et al., 2021) or by incorporating multiple cameras calibrated to enable 3D-pose triangulation from
416 multiple perspectives (Pereira et al., 2020). Second, while we used a common design for our
417 positive association assay (Colwill, 2019), other designs such as the "t_1-t_2" paradigm, in which

418 animals are first exposed to a stimulus (t_1) and learning is then assessed in a testing phase (t_2) could
419 improve the assay (Colwill, 2019). Such paradigm can guard against behavioral changes due to
420 fluctuations unrelated to the stimulus, including changes in water parameters, animals' motivation,
421 or circadian activities. Lastly, we verified that older animals were able to eat food (indicating that
422 they could generally see and move) and that there was no significant difference in average velocity
423 between young and old animals. However, we cannot exclude that more fine-tuned issues with
424 sight or movement ability may contribute to the reduced performance of older animals. Future
425 studies would need to control for these variables and increase the number of animals when
426 examining the effect of age on learning. Overall, our automated feeding system opens the door to
427 use the killifish as a scalable model to screen for genes or compounds that counter aging and age-
428 related cognitive decline.
429

430 **Acknowledgements**

431 We thank Itamar Harel, Brittany Demmitt, Robin Yeo, Ravi Nath, Adam Reeves, Xiaoai Zhao,
432 and Ariana Sanchez for scientific discussion and feedback on the manuscript. We thank Brandon
433 D. Kim for providing the raw videos to make Figure 1-video 1. We thank Robin Yeo and Xiaoai
434 Zhao for help with independent code validation. We also thank Susan Murphy, Ben Machado,
435 Rogelio Barajas, Natalie Schmahl, Jacob Chung, and Jadon Shen for their assistance with killifish
436 husbandry. Supported by RF1AG057334 (A.B.), R01AG063418 (A.B.), Stanford Brain
437 Rejuvenation Program (A.B., T.W.C), Stanford Graduate Fellowship (A.M.), a Helen Hay
438 Whitney Fellowship (C.N.B.), and a Jane Coffin Childs Fellowship (J.C.).
439

Additional Information

Competing interests: No competing interests

443 **Materials and Methods**:

444

445 **Automated fish feeding system**:

446 We designed and built an automated fish feeding system that comprises individual battery-
447 powered wireless automated feeders ("feeders"), a co-located server ("local server"), and a cloud-
448 based server ("cloud server").

449

450 We designed and built the feeders so that they can be placed on individual 2.8 L tanks supplied by
451 Aquaneering, Inc. (San Diego, CA), which are commonly used for killifish and zebrafish
452 husbandry, and fit into the tank lid's two foremost holes. The feeders can precisely deliver a fixed
453 amount of dry fish food (Otohime fish diet, Reed Mariculture, Otohime C1) repeatedly each day
454 on a highly flexible schedule. They are composed of 3D printed parts (Hatchbox PLA, 1.75 mm),
455 transparent 1/16 inch thick laser-cut acrylic (Amazon.com), nylon screws and nuts (Amazon.com),
456 a 28BYJ-48 stepper motor (Amazon.com), a Wemos D1 mini ESP8266-based development board
457 (Amazon.com), and a custom-printed circuit board (PCB) of a design ordered through OSH Park
458 (Portland, Oregon). The design incorporates a green light emitting diode (LED) and corresponding
459 photoresistor that measures food dropped and allows for automatic calibration. The 3D-printed
460 and laser cut components were designed in Autocad (Autodesk), and PCBs were designed using
461 Eagle software (Autodesk). We assembled feeders in house and programmed the ESP8266
462 microcontrollers using MicroPython language.

463

464 Feeders running MicroPython use the Message Queuing Telemetry Transport (MQTT)
465 communication protocol to connect to the local server, which acts as the MQTT broker, and obtain
466 the current time and feeding regime. Each feeder can be programmed with separate and
467 independent feeding regimes (Figure 1-figure supplement 1B). For example, for the *ad libitum*
468 regimen, the feeder was programmed to deliver 7 times per day between 7 am and 7 pm (every 2
469 hours) and to drop 5 mg of food each time. For the DR regimen, the feeder was programmed to
470 deliver 3 times per day evenly between 7 am and 9 am and to drop 5 mg of food each time. When
471 several feeders were used in parallel (one for each fish), each of the feeders was programmed
472 independently on the server. Feeders remain in deep sleep power-saving mode until their
473 designated feeding, at which point they rotate their acrylic feeding disc using the onboard stepper
474 motor from under the food hopper, in between the green LED and photoresistor array, and over
475 the drop site, before returning to the food hopper. This releases 5 mg of food per feeding while
476 measuring the resistance of the photoresistor (Figure 1-figure supplement 1A, steps 3-6), providing
477 a reportable confirmation of food delivery. The photoresistor readings for each individual device
478 are recorded on a feeding log on the server, confirming that food has dropped, or that there has
479 been a missed feeding. Missed feedings can occur for a variety of reasons, including low levels of
480 food in the hopper or the loss of communication of the feeder with the server. The feeding log
481 records feedings associated with the unique ID of a feeder, so the researcher can be alerted to the
482 issue and rectify it.
483
484 After feeding, a confirmation is relayed from the feeder to the local server, using the MQTT
485 protocol, and the confirmation is uploaded to the cloud server via an MQTT bridge. The cloud

server acts as the orchestrating database, receiving commands from the user via a Julia language-based command line interface that communicates with the underlying MQTT protocol, the SQLite database of feeder orders, the logs of feeding confirmations, and checked in feeders. This cloud server exists as an Amazon Web Service EC2 instance and relays changes from users back through the MQTT bridge to the local server and back to individual feeders, while running maintenance scripts that provide status updates on all feeders.

An overview of the system and links to the components (also listed in Figure 1-Source Data 1) is available at the github repository: https://github.com/amckay1/KilliFeeder

African turquoise killifish husbandry

All experiments were performed using the GRZ strain of the African turquoise killifish species *Nothobranchius furzeri*. Animals were housed in a 26°C circulating water system kept at a conductivity between 3500 and 4500 µS/cm and a pH between 6 and 7.5, with a daily exchange of 10% with water treated by reverse osmosis. All animals were kept on a 12-hour day/night cycle and housed within the Stanford Research Animal Facility in accordance with protocols approved by the Stanford Administrative Panel on Laboratory Animal Care (IACUC protocol # 13645).

Unless otherwise noted, animals were raised as follows: pairs of single GRZ males and single GRZ females between 1 month and 3 months of age were placed in a 2.8 L tank and allowed to breed over a 24-hour period in sand trays placed for embryo collection. After 24 hours, the trays were collected, and embryos were separated from the sand by sieving. Collected embryos were placed

in Ringer's solution (Sigma-Aldrich, 96724) with 0.01% methylene blue at 26°C in 60 mm x 15 mm petri dishes (E and K Scientific, EK-36161) at a density between 10 and 50 embryos per plate. After two weeks of monitoring, embryos were transferred to moist autoclaved coconut fiber (Zoo Med Eco Earth Loose Coconut Fiber) lightly packed in petri dishes (E and K Scientific, EK-36161) at the same density as per the previous two weeks and then incubated for another two weeks at 26°C. After two weeks on moist coconut fiber, hatching was induced by placing embryos in chilled (4°C) 1 g/L humic acid solution (Sigma-Aldrich, 53680) and incubating them in that solution overnight at room temperature. The fry was transferred to 0.8 L tanks at 2 fry per tank for the first two weeks and then 1 fry per tank for the final two weeks on the circulating system (26°C). Fry was fed freshly hatched brine shrimp (Brine Shrimp Direct, BSEP6LB) twice per day for the duration of the first four weeks post-hatching. After four weeks, adult animals who had inflated swim bladders (identified by the ability to float) were individually housed in 2.8 L tanks where they were fed Otohime fish diet (Reed Mariculture, Otohime C1). Animals were sexed at four weeks by visual inspection: males harbor vivid tail fin colors whereas females do not. Animals were placed on the automated feeding system starting at four weeks of age, with the exception of feeder-naïve animals used for the behavioral assays. The animals on feeders were fed for the entirety of the experiments using different regimens including *ad libitum* (7 feedings of 5 mg per feeding spread throughout the day), dietary restricted (3 feedings of 5 mg per feeding in the morning), and over-feeding (12 feedings of 5 mg per feeding spread throughout the day). For behavior experiments, feeder-naïve animals were fed twice a day 20 mg between 8 am and 11 am in the morning and between 2 pm and 5 pm in the afternoon during the week and once 20 mg per day between 8 am and 5 pm during weekends until they were used for the behavioral experiments.

530

531 **Comparison between automated and manual feeding**

532 To compare automated feeding with manual feeding, automated feeders were programmed to drop
533 a total of 40 mg Otohime fish diet (eight rotations of the feeding mechanism with 5 mg per
534 rotation). In parallel, individual lab members were instructed to measure out a total of 40 mg of
535 Otohime fish diet (two feeding spoons with 20 mg per spoon). The mass of each manual feeding
536 was measured using a scale to 1 mg precision. The measurement was repeated 9 times per
537 individual and a total of 19 times across 4 different automated feeders. Estimates of the standard
538 deviation both for automated and manual feedings were calculated by bootstrap using the
539 Bootstrap.jl package in Julia and then converted to precision by taking the inverse of the variance.

540

541 **Growth rate experiments and analysis**

542 All fish enrolled in a lifespan experiment were measured for size at two time points: i) young adult
543 (28 days post-hatching, which is the time of enrollment on the automatic feeders), and ii) death.
544 To avoid concerns that non-linear growth rates with older aged animals would confound the
545 analysis, only animals that lived 4 months or fewer were considered. To measure the fish size, fish
546 were placed in a clear plastic crossing tank (Aquaneering, ZHCT100T) with a water depth of 3 cm
547 and a reference ruler underneath. Images were taken using a fixed-position digital camera.
548 Analysis of size was carried out by measuring the length of the animals in pixels and converting
549 to length based upon the reference ruler's size in pixels. After animals had died (the day of or the
550 next day), dead animals were placed on a ruler and their length measured directly using a digital
551 camera. The difference in length divided by the time between the first measurement and death was

552 then reported as the fish growth rate. To accurately compare animal growth rates despite different
553 times of death, only animals that died before 4 months were compared.
554
555 Growth rates were compared between conditions using the two-sided Wilcoxon rank sum test with
556 a significance threshold alpha of 0.05.
557
558 **Fertility experiments and analysis**
559 Fish from the same hatching date at 4 weeks of age (AL and DR comparison) or 8 weeks of age
560 (AL and overfeeding comparison) were paired in 2.8 L tanks, with 1 male and 1 female. Each
561 animal was given the same feeding regime prior to enrollment: brine shrimp as described above
562 for the first 28 days post-hatching then manual feeding of Otohime C1 fish diet up until the
563 beginning of the enrollment on automated feeders. At the beginning of the enrollment, pairs of
564 males and females were crossed in the afternoon with sand trays and uncrossed ~24 hours later.
565 Pairs were crossed and uncrossed weekly on the same day and crossed until one of the pairs died.
566 Sand trays with embryos were removed at that time and sieved as described above to isolate
567 embryos, which were then rinsed and counted. The total number of embryos produced and the
568 number of fertilized embryos (indicated by separation of the chorion from the yolk membrane)
569 were recorded and reported for each pair for that week.
570
571 Fertility was analyzed between feeding conditions by treating each pairing as an independent data
572 point and using two-sided Wilcoxon rank sum test with a significance threshold alpha of 0.05.

573 Animals used for fertility assessment were part of an independent cohort from that used for the
574 lifespan and growth rate evaluation.
575
576 **Lifespan experiments and analysis, including Gompertz curve estimation**
577 Embryos for lifespan experiments were produced as described above. Briefly, GRZ males and
578 females were bred overnight, with embryos placed in Ringer's solution for two weeks at 26°C and
579 on coconut fiber for another two weeks at 26°C before being hatched in humic acid. Any animals
580 that did not hatch were censored and removed from the experiment. Fry that hatched were
581 transferred to 0.8 L tanks were split on the strict timescale previously described: two fry per 0.8 L
582 tank for the first 2 weeks post-hatching, and then one fry per 0.8 L tank for the subsequent 2 weeks
583 post-hatching. After 4 weeks post-hatching, adult individuals were individually placed in 2.8 L
584 tanks for the remainder of their lives. When placed in 2.8 L tanks, animals were transferred to
585 feeding with Otohime C1 fish diet using an automated feeder. Both males and females were used
586 for lifespan experiments unless otherwise stated, sex determined by the bright coloring of the male
587 tail fins. Animals were checked daily and animals that died were recorded as dying on the day
588 found. Two cohorts in total were aged, animals from each cohort being from the same breeding
589 pairs and enrolled into the cohort based upon hatch date. Any animals whose automated feeders
590 stopped performing due to damage to the feeder were censored.
591
592 Statistical analysis of lifespan experiments was conducted using the Logrank test with a
593 significance threshold alpha of 0.05. We also analyzed lifespan data with the Cox proportional
594 hazard model controlling for hatch date (with a significance threshold of 0.05). Gompertz curves

were calculated using the combined males from both cohorts 1 and 2. Briefly, males on dietary restriction or *ad libitum* feeding regimes were pooled and a Gompertz distribution fitted to the two groups using the R *flexsurv* library and the *flexsurvreg* function with a "Gompertz" distribution. The resulting estimated parameters for the intercept and slope of the Gompertz curve were then plotted in Julia using a custom script. Estimates for the hazard rate were assessed by calculating the hazard function based upon 3-week binning of mortality rates for the two groups, dietary restricted males or *ad libitum* males. Gompertz curve parameter estimates reported with estimated 95% confidence levels.

Fish cohort and tissue dissection for RNA-seq experiment

All fish were raised from embryos collected from 15 male-female pairs, when these breeders were 9-10 weeks of age (within their reproductive peak). Collected embryos were treated with mild iodine (0.2%, diluted from Povidone-iodine solution (10% w/v, 1% w/v available iodine, RICCA #3955-16)) on Day 1 to reduce contamination, incubated in embryo solution with 0.01% methylene blue (Kordo, #37344), and then placed on moist coco fiber on the 14th day after collection. After two weeks on coco fiber, fish were hatched in ~1 cm-deep cold 1 g/L humic acid solution, at room temperature. For the next four days, the fish were housed on the countertop of the animal facility at 25°C. System water was added to the hatching containers, and fish were fed live brine shrimp daily. For the following 2 weeks, fish were housed at a density of 4 fish per 0.8 L tank and fed with brine shrimps daily. In the following 2 weeks, housing density was reduced to 2 fish per 0.8 L tank and fish were fed as before. Each fish was first imaged from the top using a digital camera

617 at a fixed position and then transferred to a 2.8 L tank. Lastly, an automatic feeder was put on each
618 tank, and either AL or DR feeding regime was assigned randomly to each fish. Feeders were
619 programmed according to this random assignment. Metadata for the animals used in this
620 experiment can be found in Figure 5-Source Data 1.
621
622 Brains and livers were harvested from these killifish in two batches on two days (4 males and 4
623 females on each day), when the fish were 9 weeks of age and had been subjected to the assigned
624 diet regimes for 5 weeks. Fish were randomly assigned to a harvest batch, with each batch having
625 2 fish from each condition (AL-Male, DR-Male, AL-Female, DR-Female). On harvest day, the
626 automatic feeders were first removed from the tank. Next, 1.5 h after the light turned on, for AL
627 treatment, fish were manually fed 17.5 mg of dry food; and for DR treatment, fish were fed 7.5
628 mg of dry food. This quantity of food corresponded to half of the total daily food amount and
629 maintained the differential ratio of food intake for the two diet regimens. From 12 PM to 3 PM, 8
630 fish were euthanized on ice, and organs were extracted and snap-frozen in liquid nitrogen. All
631 organs were stored at -80˚C until RNA isolation.
632
633 **RNA isolation, cDNA library generation, and sequencing**
634 We isolated RNA from liver and brain using Qiagen RNeasy Mini kit (Qiagen, #74106) according
635 the manufacturer's instructions. The processing order of each organ was randomized. The tissues
636 were transferred to the 1.2 mL Collection Microtubes (Qiagen, #19560) on dry ice in a 4°C cold
637 room to reduce tissue thawing. Next, an autoclaved metal bead (Qiagen, #69997) and 700 µL of
638 QIAzol (Qiagen, #79306) were added to each tube. Two rounds of tissue homogenization were

639 performed on the TissueLyserII machine (Qiagen, #85300) at 25 Hz, 5 min each, at room
640 temperature. The lysate was transferred to new 1.5 mL tubes, 140 µL chloroform (Fisher Scientific,
641 #C298-500) was added, and the tubes were vortexed for 15 sec. After incubation at room
642 temperature for 2-3 min, lysates were centrifuged at 12,000 x g at 4°C for 15 min. The aqueous
643 phase was mixed with 350 µL ethanol (200 Proof, Gold Shield Distributors, #412804) by inverting
644 the tubes 10 times. The mixture was transferred to the RNeasy column, washed with 350 µL RW1
645 buffer (provided by the RNeasy Mini kit), and treated with DNase I (following the kit's protocol)
646 at room temperature, for 15 min. The column was washed 2 times with 500 µL RPE buffers, and
647 the RNA was eluted with 50 µL nuclease-free water (Invitrogen, #10977023). RNA quality and
648 concentration were measured using an Agilent 2100 Bioanalyzer and the Agilent Nano Eukaryotic
649 RNA Kit (Agilent, #5067-1511). All bioanalyzer assays were performed by the Stanford Protein
650 and Nucleic Acid Facility.
651
652 Next, cDNA synthesis was performed using the Takara SMART-seq v4 PLUS kit (Takara,
653 #634889) according to the manufacturer's instructions. Briefly, 10 ng of RNA from each sample
654 was incubated with 1 µL of 10x Reaction Buffer and 2 µL of CDS primer IIA in a 12.5 µL reaction,
655 at 72°C, for 3 min. Next, each sample was mixed with 7.5 µL RT Master Mix (4 µL 5x Ultra Low
656 First-Strand Buffer, 1 µL SMART-Seq v4 48 µM Oligonucleotide, 0.5 µL 40 U/µL RNAse
657 inhibitor, and 2 µL SMARTScribe II Reverse Transcriptase), incubated at 42°C for 90 min and
658 then 70°C for 10 min. To amplify the cDNA, each sample was mixed with 30 µL of PCR Master
659 Mix (25 µL SeqAmp PCR Buffer, 1 µL PCR Primer II A, 3 µL nuclease-free water, and 1 µL

SeqAmp DNA Polymerase) and PCR-amplified for a total of 8 cycles. The amplified cDNA (a total of 30-50 µL) was purified using 90 µL Beckman Coulter AMPure XP beads (Beckman Coulter, #A63880) following the manufacturer's guideline, including 2 washes of 200 µL 80% ethanol (200 Proof, Gold Shield Distributors, #412804; diluted in nuclease-free water), and elution in 40 µL of nuclease-free water (Invitrogen, #10977023). The concentration and quality of the amplified cDNA library were measured using the Agilent 2100 Bioanalyzer and Agilent's High Sensitivity DNA Kit (Agilent, #5067-4626) by the Stanford Protein and Nucleic Acid Facility.

The cDNA libraries were prepared using the Illumina NexteraXT DNA library prep kit (Illumina, #FC-131-1096) based on the manufacturer's protocol. Briefly, for tagmentation, 0.5 ng of the cDNA (5 µL total) was mixed with 10 µL TD buffer and then 5 µL ATM buffer from the Nextera kit. Each reaction was incubated at 55°C for 4 min and then cooled to 10°C. To stop the tagmentation reaction, 5 µL of NT buffer was added immediately and incubated with the reaction mixture at room temperature for 5 min. The Illumina Nextera XT Index Kit v2 (Illumina, #131-2001) was used for library indexing. The cDNA library was indexed and amplified for a total of 13 cycles in a PCR reaction that contained the 20 µL of tagmented DNA, 5 µL of i7 adaptor, 5 µL of i5 adaptor, and 15 µL NPM buffer. The amplified cDNA library (50 µL total) was purified using 90 µL of Beckman Coulter AMPure XP beads as described above and eluted in 52.5 µL RSB buffer. The concentration and quality of the library were measured using the Agilent 2100 Bioanalyzer and Agilent's High Sensitivity DNA Kit (Agilent, #5067-4626) by the Stanford Protein and Nucleic Acid Facility.

682 The cDNA library was sequenced on an Illumina NovaSeq 6000, PE150 platform by Novogene
683 (Novogene, Beijing, China), at a sequencing depth of >20 million pair-end reads. We noted that
684 some of the samples were sequenced on a separate flow-cell, which were indicated in the
685 "sequencing batch" column of the sample metadata file.
686
687 **Sequencing quality control and read mapping**
688 Raw sequencing data (FASTQ files) were processed and checked for quality using Trim-galore
689 v0.4.5. The processed reads were aligned to the African turquoise killifish reference genome
690 downloaded from NCBI (Nfu_20140520, GCF_001465895.1). The read alignment was performed
691 using STAR v2.7.1a (Dobin et al., 2013) with the default parameters. Out of 32 RNA-seq samples,
692 15 samples had >90% of reads mapped to the genome; 10 samples, 80-90% reads mapped; and 7
693 samples, 75-80% mapped. Next, we used samtools v1.5 (Li et al., 2009) to remove the reads that
694 map to multiple genomic regions, using the parameters of MAPQ<255 ("samtools view -q255 -
695 b"). These uniquely mapped reads were then used to generate the read counts for each gene, for
696 which we used the "featureCounts" program from subread v2.0.1 (Liao et al., 2014) using the
697 default parameters.
698
699 **DEseq2 analysis**
700 We used DESeq2 v1.32.0 (Love et al., 2014) to analyze the differential gene expression as follows.
701 First, a pseudocount of "1" was added to all the read counts. Next, the "dds" object was created
702 using the parameter "design = ~Condition", where "Condition" is a compound variable specified

by "tissue_sex_diet". The genes were filtered such that those with fewer than 15 counts (i.e., cutoff equals 16 due to pseudocount of "1") were removed from the "dds" object.

Principal Component Analysis (PCA) was performed by first applying the variance stabilizing transformation ("vst") on the "dds" object and then visualizing using ggplot2 v3.3.5. To generate the PCA plot for a given tissue, the count matrix (already added a pseudocount of "1") was first subsetted so that only the samples for that tissue remained.

Diet DEGs and sex DEGs for the liver

Because tissue identity was the main contributor of the variation among samples (as expected), we performed the DESeq2 analysis for only the liver samples, which allowed us to identify more subtle gene expression changes that might be explained by sex and/or feeding regimen. For the brain samples, one AL sample was located 3 standard deviations away from the rest of the samples in PC1. We thus excluded this sample from the PCA plots.

To identify the diet-differential expressed genes (diet DEGs) for the liver, we used the tissue-subsetted "dds" object created above ("design = ~Condition") and extracted the DEGs between the AL (reference) and DR samples, separately for males and females, using the "contrast" parameter of the "results" function in DESeq2 (Figure 5-Source Data 2, 3). We used the two gene lists, separately, as the input for the Gene Set Enrichment Analysis (GSEA) below.

To identify the sex-differential expressed genes (sex DEGs) for the liver, we extracted the DEGs between males and females under the AL or DR condition, again using the "contrast" parameter

of the "results" function in DESeq2 (Figure 5-Source Data 4, 5). There were 1081 sex DEGs in AL and 2151 sex DEGs in DR ($p < 0.05$), with 743 genes shared by the two conditions.

Lastly, we identified the diet-sex interaction genes by creating a "dds" object for the liver using "design = ~diet + sex + diet:sex", removing genes with fewer than 15 counts (i.e., cutoff equals 16 due to pseudocount of "1"), and running the "DEseq" function with the "female AL" condition as a reference. A positive log2-transformed fold change (log2FC) occurs when the ratio of DR/AL is higher in males than in females; a negative log2FC occurs when the ratio of DR/AL is lower in males than in females. There were 12 significant diet-sex interaction genes (Figure 5-Source Data 10). While this number of genes is too low for GO enrichment analysis, these genes are involved in immune-related, lipid metabolism, and intracellular trafficking function, consistent with the GSEA results.

To visualize the expression distribution (Figure 5-figure supplement 1C), we used the "plotMA" function in DEseq2 to make a scatterplot for the log2 fold change and the log10 of the mean normalized counts.

Enrichment of sex DEGs in diet DEGs

We calculated the enrichment of the sex DEGs (identified either in AL or in DR) in diet DEGs as follows. First, we removed the genes with an "NA" value for the p.adjust in any dataset, and then we created a contingency table (for males and females separately) by counting the genes that satisfied the following categories: (1) group 1: genes differentially expressed by both sex and diet

747 (i.e., sex DEGs with p.adjust < 0.05 and diet DEGs with p.adjust < 0.05); (2) group 2: genes
748 differentially expressed only by sex (i.e., sex DEGs, p.adjust < 0.05) and not by diet (i.e., diet
749 DEGs, p.adjust ≥ 0.05); (3) group 3: genes differentially expressed only by diet (i.e., diet DEGs,
750 p.adjust < 0.05) and not by sex (i.e., sex DEGs, p.adjust ≥ 0.05); and (4) group 4: genes not
751 differentially expressed by diet or sex (i.e., diet DEGs with p.adjust ≥ 0.05 and sex DEGs with
752 p.adjust ≥ 0.05). In Figure 5E and Figure 5-figure supplement 1E, the enrichment was defined as
753 the ratio of group 1 gene number over the number of diet DEGs (i.e. (group 1)/(group 1 + group
754 3)). Because the two sexes were analyzed separately in the DEseq2 analysis, two contingency
755 tables were created—one for male diet DEGs and one for female diet DEGs. A two-tailed Fisher's
756 exact test was used to calculate the statistical significance of the enrichment.
757
758 Non-diet DEG control gene sets (one for either sex) were generated to control for any bias in gene
759 expression distribution and gene group size of the diet DEGs. To do so, for each diet DEG, we
760 identified all the non-diet DEGs that were within 2% of the diet DEG's average expression level
761 (average across all samples). When the expression threshold was set at 1%, one diet DEG had no
762 associated control gene; thus, an expression threshold of 2% was selected. These genes constituted
763 the "non-diet DEG control group" for a given diet DEG. Next, we randomly selected 1 gene from
764 each non-diet DEG control group, for all 221 of the female diet DEGs and 70 for the male diet
765 DEGs. These randomly selected genes comprised the control gene set, which had the same number
766 of genes as the diet DEGs. To perform a boostrapped analysis, we generated 1000 control gene
767 sets and tested each of them for sex DEG enrichment by a two-tailed Fisher's exact test. We plotted

768 the median enrichment and the median p-value (Fisher's exact test) of these 1000 iterations. All
769 pie-charts were plotted in R v4.1.0. The bootstrap data can be found in Figure 5-Source Data 11.
770
771 **Gene set enrichment analysis (GSEA)**
772 We performed GSEA (Mootha et al., 2003; Subramanian et al., 2005) as follows. First, for a given
773 gene list (male diet DEGs and female diet DEGs), we sorted all transcripts in descending order
774 based on their ranked scores, which were calculated by multiplying the -log10(p-value) with log2
775 fold change. Genes without p-values reported from DEseq2 analysis were removed. Next, we
776 identified the human ortholog name for each killifish gene via protein blast (best hit protein with
777 BLASTp E-value >1e-3). If multiple killifish paralogs were blasted to the same human gene, the
778 average of the ranked scores was calculated and assigned to this human gene name. If no human
779 ortholog was found, this killifish gene was removed from the gene list. Lastly, we ran the
780 enrichment analysis via clusterProfiler v4.0.5 (Yu et al., 2012) and the Bioconductor annotation
781 data package ("org.Hs.eg.db" v3.13.0) and GOstats package (v2.58.0). The p-values of the
782 enriched pathways were corrected for multiple hypotheses testing using the Benjamini-Hochberg
783 method (p.adjust). A Gene Ontology (GO) term was considered significantly enriched if it had a
784 p.adjust value < 0.05. The top 5 GO terms from the "male diet DEGs" and "female diet DEGs"
785 gene lists were graphed as a dot plot. The full GSEA data are in Figure 5-Source Data 6, 7.
786
787 **Hypergeometric gene ontology (GO) enrichment analysis**
788 We used the "GSEABase" (v1.54.0) and GOstats (v2.58.0) packages for this analysis. For male
789 diet DEGs and female diet DEGs, we first separated these two diet DEG lists (p.adjust < 0.05)

based on upregulation or downregulation in DR. The resulting 4 gene lists were individually used for the hypergeometric test implemented in GOstats (v2.58.0). For the sex DEGs identified in AL and those identified in DR, we separated these two sex DEG lists based on upregulation or downregulation in males. Each of the 4 gene lists was used for the hypergeometric test. The background genes ("universe") were defined as all of the genes with a non-NA value for p.adjust for a given comparison. The full GO analysis results are in Figure 5-Source Data 8, 9.

We found that protein homeostasis (e.g., "ERAD pathways") and intracellular trafficking (e.g., "protein glycosylation") GO terms were significantly enriched in the female diet DEGs upregulated in DR (Figure 5-figure supplement 1D). In contrast, lipid metabolism (e.g., "fatty acid biosynthetic process") GO terms were enriched in the female diet DEGs downregulated in DR. For males, intracellular trafficking GO terms (e.g., "regulation of protein secretion") were also significantly enriched in the diet DEGs upregulated in DR, but the enrichment score was lower than for females. Lipid metabolism GO terms were also enriched in the diet DEGs downregulated in DR in males, but both the enrichment score and the statistical significance were lower than for females. Thus, the specific upregulation of protein homeostasis pathways in female DR livers and the downregulation of lipid metabolism in female DR livers (to a greater extent than in males) are consistent with the GSEA results.

Lastly, GO analysis on the sex DEGs identified in AL showed that the genes more highly expressed in AL male livers were enriched in cellular amino acid catabolic processes and gluconeogenesis pathways. In contrast, genes more highly expressed in AL female livers were enriched in estrogen

response, humoral immune response, and female sex differentiation. GO analysis on the sex DEG identified in DR showed that while most GO terms were similar to those for the AL sex DEGs, protein homeostasis pathway (e.g., "ER stress response") was uniquely enriched in the genes more highly expressed in DR female livers. This observation is consistent with our results from GSEA and GO analysis on the diet DEGs.

Heatmap

Heatmaps were generated using Pheatmap (v.1.012). We identified the killifish orthologs for all the human genes associated with each GO term. For each killifish ortholog gene in the GO term, we subjected the normalized counts generated from the DEseq2 analysis to the following. First, we calculated the mean and standard deviation (SD) across all the replicates (n = 4 for AL; n = 4 for DR) of the selected gene. Next, we scaled each normalized count value (x_i) by $z_i = (x_i - \text{mean})/SD$ and used z_i as the input for heatmaps. Hierarchical clustering was performed using Pearson correlation and "ward.D2" method (hclust(as.dist(1-cor(t(allCounts_GeneGO_plot_f))), method = "ward.D2")). Heatmaps were plotted using the distance matrix (from clustering) and the parameters (clustering_method = "ward.D2", treeheight_row = 0, treeheight_col = 1, cluster_cols = F, cluster_rows = T).

Fish cohorts for the associative learning assay

Animals were raised as described above, except that GRZ pairs were crossed for a longer duration (up to one week) before embryo collection. The animals were raised to adulthood with less stringent density requirements: 4-5 fry were placed per 0.8 L tank for 2-3 days before being split

834 to 2 fry per tank for the remainder of the four weeks before sexual maturity. After sexual maturity,
835 fish were individually housed in 2.8 L tanks. For these experiments, fish were manually fed as
836 previously described ("feeder-naïve") and consisted of males (n = 17) and females (n = 10) with
837 age ranging from 36-days to 130-days post-hatching. Metadata for the animals used in this
838 experiment can be found in Figure 6-Source Data 1.
839
840 **Associative learning assay**
841 Animals were transferred from their home tanks to designated behavioral tanks (on a different
842 rack) in batches, with individuals selected for each batch chosen at random. Individual tanks were
843 separated from one another using white foam-core sheets. The tanks on the behavior rack received
844 recirculating water from the system as did the home tanks.
845
846 Each experiment consisted of 17 trials conducted across 3 consecutive days, with 7 trials for the
847 first 2 days and 3 trials on Day 3. On Day 0 (the day before the first trial), animals were placed in
848 individual behavior tanks in the afternoon after receiving their afternoon manual feeding. Each
849 automated feeder used for the behavioral assay had an additional red LED light that served as the
850 conditioned stimulus and was installed adjacent to the feeding hole. This red LED light is
851 programmed to turn on and off by the same Julia language-based command line interface that
852 communicates with MQTT protocol that sends feeding commands to each feeder. We programmed
853 the automatic feeders to initiate the first session of stimulus presentation and feeding on Day 1 at
854 7 AM. For the sessions on Days 1-3, the feeders were programmed to run the sessions

855 autonomously. On Day 4, animals were removed from behavior tanks and placed in their home
856 tanks, and normal feeding and care resumed.
857
858 Videos were recorded using an ESP32-CAM module from the anterior of the tank. The sequence
859 of events recorded was as follows: (1) Camera turned on, (2) on the 2nd second, the red LED light
860 turned on, (3) on the 9th – 11th second, the food arrived at the water surface, and (4) camera
861 remained on during feeding and ended >10 seconds after food dropping. In sum, animals were
862 trained with a conditioned stimulus (red light) delivered 7 seconds before the unconditioned
863 stimulus (food, 5 mg dropped at a time). Videos were analyzed by manual scoring and automated
864 tracking. Out of the 27 fish tested in this assay, 11 fish were excluded due to technical issues
865 (camera failed to record all 17 trials for 5 fish, and feeders failed to drop food for 6 fish). Three
866 fish displayed eating behavior in fewer than 3 trials, and they often stayed at the bottom of the
867 tanks and rarely moved. We considered that these fish potentially had underlying health issues,
868 lacked motivation for food, and/or failed to adapt to the videotaping tanks. Thus, we excluded
869 these animals from our analysis. Altogether, a total of 13 animals were analyzed (9 males and 4
870 females).
871
872 **Automated analysis of the associative behavior assay using DeepLabCut**
873 Automated tracking was performed by DeepLabCut 2.2 (Mathis *et al.*, 2018), an open-source deep-
874 learning tracking software, and the output data were analyzed using custom R and Julia scripts.
875 Briefly, the DeepLabCut software was trained on representative annotated training video frames
876 (20 frames/second; the given number of videos annotated was set by the default setting in

877 DeepLabCut) using a transfer learning approach as follows: Superficial layers of the neural
878 network were updated while the core ResNet-50 layers were left untouched, resulting in relatively
879 rapid training of the network. All killifish training videos were processed using this network.
880 DeepLabCut results were exported as CSV files, providing the x- (side-to-side in tank) and y- (top-
881 to-bottom in tank) coordinates and likelihood values for fish snouts, fish tails, the food drop site,
882 and the red training light. Tracked videos varied slightly in length, but minimally were 18 seconds
883 long (360 frames).
884
885 Several prefiltering steps were performed on these positional values as follows: (1) First, fish head
886 likelihood values were selected if they passed the threshold of 0.999, meaning that the coordinates
887 for the frames with likelihood values < 0.999 were set to "NA" (leading to exclusion of 41,623
888 frames). (2) Second, of the selected coordinates, the Euclidean distance between the x,y positions
889 from contiguous frames was calculated for all frames and for all videos. If the Euclidean distance
890 between any two contiguous frames was in the top 5% of all distances calculated, this was
891 considered an anomaly. The coordinates of the second frame of the two contiguous frames was set
892 to "NA" (after this step, 10,051 additional frames were filtered out). (3) Lastly, given that the
893 previous filtering steps led to missing positional values in the data ("NA"), the final processing
894 step was interpolation. We performed interpolation using the na.spline function in the zoo R
895 package (version 1.8-10). The na.spline function performs cubic spline interpolation, which
896 involves finding low-degree polynomial curves that connect data points and results in smooth,
897 continuous values and matching first and second derivatives where the polynomial curves meet.
898 We did not perform any extrapolation, so some "NA" values did remain where an unknown value

was not preceded or followed by a known value, for example in cases where there were long stretches of "NA" in the beginning or the end of a video. The resulting data were used for velocity calculations and plotting of movement trajectories. All the unfiltered raw trajectory data can be found in the file Figure 6-Source Data 2 and the filtered and interpolated trajectory data with kinematics calculations can be found in the file Figure 6-Source Data 3.

Automated scoring and trajectory analysis

The prefiltered and interpolated coordinates were used to calculate the instantaneous velocity in the y-direction (up-down in the tank) for each frame. Rolling averages of the instantaneous velocities were calculated over 20 frames using the zoo package, and then the raw velocity of each frame was adjusted to the 20-frame rolling average. This adjustment allowed us to better visualize the regions of increased activity. We plotted the velocities as heatmaps. For the velocity heatmap, the top 7% and bottom 10% of velocities are set as the extremes on the heatmap color scale. We also used the coordinates to determine the Euclidean distance of the fish from the coordinates of where food drops for each frame. For each fish, the location of where food drops on the water surface was determined by taking the average of the highest likelihood food drop coordinates across all videos for that animal.

We calculated t_1 by (1) determining the beginning and end times of the "bursts" of velocity activity (yellow regions in Figure 6) for each animal in each trial and (2) determining the times during each trial when the fish was "arriving at the surface". We set the threshold for a high velocity burst for each animal as approximately the top 25% of the velocity range and the threshold for arriving at

921 the surface was defined as 100-150 pixels away from the food drop location (see Figure 6-Source
922 Data 4). The t_1 values were calculated by finding the closest velocity burst to a time of arrival at
923 the surface and using the beginning time of the velocity burst as the t_1. If the fish never arrived at
924 the surface during a trial, the t_1 would be set to 18 seconds. If the fish began the trial at the surface,
925 the t_1 would be set to 0 seconds. In 3 trials (out of 221 trials for all fish), the velocity thresholds
926 were set slightly too high, and the velocity bursts were determined by inspecting the velocity
927 heatmap manually (see Figure 6-Source Data 4 for details). Finally, we calculated the Pearson
928 correlation between the automated t_1 values and the manual t_1 values using Prism v.9.3.1.
929
930 Fish x-y trajectories (in pixel space) were plotted using the fish head coordinates and were shown
931 relative to the locations of food delivery (calculated as the average of all the high-likelihood
932 locations) and the red light (calculated as the average of all the high-likelihood locations). The
933 trajectory of the fish was colored by time, with the blue representing the fish location at 2 seconds
934 and yellow, at 9 seconds. The trajectories from trial 4 and trial 17 for Fish 3 were plotted. Plots
935 were made using the "geom_path()" function in R. All the data related to automatic quantification
936 can be accessed in Figure 6-Source Data 4.
937
938 **Compass plot**
939 A compass plot displays the angle of a velocity vector, showing the fish's direction of movement
940 between the initial position (when the light turns on at 2 seconds) and the final position (when
941 the food drops at 9 seconds). The compass plots shown in Figure 6-figure supplement 1A are the
942 frequency distribution of the angular coordinates (see below) for all the velocity vectors that

were annotated for all the fish in the first 7 trials, or annotated for all the fish in the last 7 trials. To generate these plots, we first determined the initial position of the fish after the red light turned on (2 seconds) and the final position of the animal when the food was dropped (9 seconds). Next, we converted these positions from Cartesian coordinates (x, y) to polar coordinates (r, θ). Lastly, we converted the angular coordinate (θ) of the vector (from the initial position to the final position) from radians to degrees. The angular coordinates (θ) from the first 7 trials (or the last 7 trials) for all the fish were pooled and then binned to create a frequency distribution (bin size = 20°, histograms centered on midpoint of bin) that could then be plotted as a compass graphs using the "coord_polar()" function in R. Each "wedge" on the compass plot represents a bin. The wedge is directed toward the angle (out of 360º) that corresponds to the midpoint of the bin, and has a radius that indicates the frequency of angles in the bin (larger radius indicating that more velocity vectors fallen into that bin). All the velocity-vector bins have the same origin. All plots were generated using ggplot2 in R. All data for input into the compass plots can be found in the file Figure 6-Source Data 5.

Manual analysis of the associative behavior assay

For manual analysis, each video (one trial) was analyzed second-by-second, and three metrics were tracked for each second: (1) Did the midpoint of the fish have a positive y-axis displacement during this second? A score of "1" was given if the y-axis displacement was greater than 0 (i.e. the fish moved toward the water surface); otherwise, a score of "0" was given (i.e. the fish moved away from the water surface or stayed at the same water level). (2) Was the fish at the water surface? A

964 score of "1" was given if the fish's snout was within ~0.5 cm of the water surface (the fish's
965 reflection was visible); otherwise, a score of "0" was given. (3) Was the fish eating the food? If
966 so, "eating" was noted for this second.
967
968 For each fish, we graphed metric 1 and 2 scores against time, respectively (Figure 6-figure
969 supplement 1B). We identified the first time at which the fish reached the water surface, and then
970 we backtracked when the fish initiated a continuous trajectory toward the surface (i.e. identifying
971 when the string of "1" in the y-axis displacement plot began). This initiation time of the first
972 surface-bound trajectory is defined as "t_1." Sometimes, the fish would stop moving for ≥1 second
973 during its ascent to the surface. In this case, we disregarded this first part of ascension and reported
974 t_1 to be the initiation time of the second part of the ascent, during which the fish had a continuous
975 upward trajectory and ultimately reached the surface. Our measurement in this scenario are likely
976 conservative, and it is possible that the fish moved toward the water surface earlier than what we
977 reported here.
978
979 To measure how robust our method is for determining t_1, 3 researchers (E.K.C., J.C., R.C.K.)
980 independently analyzed the same set of 17 videos from one fish. The results were consistent across
981 all 3 researchers, with a Pearson correlation of >0.95 for any pair-wise comparison, suggesting
982 that this analysis method is robust against the subjective judgment of observers.
983
984 **Quantification of successful association**

We defined a successful trial to be when the fish initiated its surface-bound trajectory (t_1) before food drop. Thus, a successful trial would be the one with $2 \leq t_1 \leq 9$, where "2" corresponded to when the light turned on at 2 seconds, and "9" corresponded to when the food arrived on the water surface at 9 seconds. We noted that there was some variability to when the food arrived (the food was set to dropped at 5 seconds, but there were network and mechanical delays), ranging from 9-11 seconds. Thus, the window of success (2-9 seconds) should be considered conservative.

To quantify successful association, we calculated the average t_1 for the first 7 trials ("early trials") and the last 7 trials ("late trials") for each fish. The average t_1 values for all the fish, or for young and old fish, were plotted as a dot plot overlaid on a box plot, where each fish was denoted as a unique symbol. In the automated quantification method, for two animals (Fish 13 and 14), the t_1 of Trial 7 was not calculated due to low-likelihood position values, and the average t_1 of the early trials was calculated using the first 6 trials.

In another metric to measure successful association, we calculated the number of successful t_1, which fell in the range of 2 to 9 seconds (including 2 and 9) for the early and late trials, respectively, for each fish. The percentage of success was calculated as the number of successful t_1 divided by 7. The values of the average t_1, as well as the percent success, for the early trials and the late trials for the same fish were considered as a matched pair for the two-tailed Wilcoxon matched-paired signed rank test. All the graphs and statistics were performed in Prism v9.3.1.

Learning index

We defined the "learning index" as the inverse of the first trial number needed for an animal to achieve a given number of consecutive successes. This metric treats the trials as dependent on one another to reflect that the prior experiences of an animal can influence future performance. We took the inverse of this first trial number to make "faster association" be a higher learning index value. As an example, for Fish 3 (Figure 6E), its learning index corresponded to the first trial when 2 consecutive successful trials occurred. In this case, trial 4 was the first time when $2 \leq t_1 \leq 9$ for two consecutive trials (both trials 4 and 5 were successful). Thus, the "learning index" would be 1/4 (0.25). Most of the killifish (85%) can achieve 2 consecutive successes, while only 54% and 38% can achieve 3 or 4 consecutive successes, respectively (Figure 6-Source Data 6, "learning index_3" and "learning index_4"). Thus, the number of consecutive successful trials reveals the fish-to-fish variation in the association performance across trials, a useful metric for examining the behavior stability of individual fish.

Prism v.9.3.1 was used to generate all dot plots, scatterplots, and Pearson correlation calculation. All the data related to manual quantification can be accessed in Figure 6-Source Data 6, 7, 8.

Average velocities for young vs. old fish

To calculate the average velocities for each fish, we used the calculated 20-frame rolling average velocities for each frame (see details above). We set the top and bottom 15% of velocities for a given animal to one of two boundary values – the top 15% percentile velocity or the lowest 15% percentile, respectively. Thus, the values outside of the middle 70% were capped to the boundary values. This thresholding prevents the average values from being skewed by poor velocity

estimation from the frames with low likelihood values. We used the average of all the 20-frame rolling average velocities across all the frames and all trials for a given animal.

Cohen's d effect size calculation

We calculated the standardized mean difference (Cohen's d = (mean x1 – mean x2) / standard deviation), cohen.d() and 95% confidence intervals in R. Using this, the effect size estimate of the learning index calculated from the automated analysis pipeline is -0.7862264 with a confidence interval of (-2.0860663, 0.5136134), grouping both sexes. This is ~1 standard deviation between the two group means.

Power analysis

Grouping both sexes, the mean and standard deviation of the young group (47-70 days of age post hatching) and the old group (119-130 days of age post hatching) were calculated. Power analysis was performing using G*Power (v.3.1.9.6) with the following parameters: test family: "t-tests"; statistical test: "Means: Wilcoxon-Mann-Whitney test (two groups)"; type of power analysis: "A priori: Compute required sample size – given α, power, and effect size"; tail(s): "Two"; parent distribution: "Normal"; effect size d: "-0.7862264" for learning index (Cohen's d), and "0.8046403" and "0.3544401" for the difference in t_l and in the percentage of success, respectively, between the first and last 7 trials (both effect sizes were calculated in G*Power using the mean and standard deviation of the two age groups); α error prob: "0.05"; Power (1-β err prob): "0.8"; and Allocation ratio N2/N1: "1".

Code is available in Github repository (https://github.com/emkcosta/KillifishAutomaticFeederPaper/).

References

Ahuja, G., Bartsch, D., Yao, W., Geissen, S., Frank, S., Aguirre, A., Russ, N., Messling, J.E., Dodzian, J., Lagerborg, K.A., et al. (2019). Loss of genomic integrity induced by lysosphingolipid imbalance drives ageing in the heart. EMBO Rep *20*. 10.15252/embr.201847407.

Api, M., Notarstefano, V., Olivotto, I., Cellerino, A., and Carnevali, O. (2018). Breeders Age Affects Reproductive Success in Nothobranchius furzeri. Zebrafish *15*, 546-557.

Bagnoli, S., Fronte, B., Bibbiani, C., Terzibasi Tozzini, E., and Cellerino, A. (2022). Quantification of noradrenergic-, dopaminergic-, and tectal-neurons during aging in the short-lived killifish Nothobranchius furzeri. Aging Cell *21*, e13689. 10.1111/acel.13689.

Bartke, A., Wright, J.C., Mattison, J.A., Ingram, D.K., Miller, R.A., and Roth, G.S. (2001). Extending the lifespan of long-lived mice. Nature *414*, 412. 10.1038/35106646.

Baumgart, M., Di Cicco, E., Rossi, G., Cellerino, A., and Tozzini, E.T. (2015). Comparison of captive lifespan, age-associated liver neoplasias and age-dependent gene expression between two annual fish species: Nothobranchius furzeri and Nothobranchius korthause. Biogerontology *16*, 63-69. 10.1007/s10522-014-9535-y.

Bonkowski, M.S., Rocha, J.S., Masternak, M.M., Al Regaiey, K.A., and Bartke, A. (2006). Targeted disruption of growth hormone receptor interferes with the beneficial actions of calorie restriction. Proceedings of the National Academy of Sciences of the United States of America *103*, 7901-7905. 10.1073/pnas.0600161103.

Brandhorst, S., Choi, I.Y., Wei, M., Cheng, C.W., Sedrakyan, S., Navarrete, G., Dubeau, L., Yap, L.P., Park, R., Vinciguerra, M., et al. (2015). A Periodic Diet that Mimics Fasting Promotes Multi-System Regeneration, Enhanced Cognitive Performance, and Healthspan. Cell Metabolism *22*, 86-99. 10.1016/j.cmet.2015.05.012.

Bronikowski, A.M., Meisel, R.P., Biga, P.R., Walters, J.R., Mank, J.E., Larschan, E., Wilkinson, G.S., Valenzuela, N., Conard, A.M., de Magalhaes, J.P., et al. (2022). Sex-specific aging in animals: Perspective and future directions. Aging Cell *21*, e13542. 10.1111/acel.13542.

Broza, M., and Halpern, M. (2001). Pathogen reservoirs. Chironomid egg masses and Vibrio cholerae. Nature *412*, 40. 10.1038/35083691.

Cellerino, A., Valenzano, D.R., and Reichard, M. (2016). From the bush to the bench: the annual Nothobranchius fishes as a new model system in biology. Biological Reviews *91*, 511-533. 10.1111/brv.12183.

1095 Cho, C.E., Brueggemann, C., L'Etoile, N.D., and Bargmann, C.I. (2016). Parallel encoding of
1096 sensory history and behavioral preference during Caenorhabditis elegans olfactory learning. Elife
1097 *5*. 10.7554/eLife.14000.

1098 Colman, R.J., Anderson, R.M., Johnson, S.C., Kastman, E.K., Kosmatka, K.J., Beasley, T.M.,
1099 Allison, D.B., Cruzen, C., Simmons, H.A., Kemnitz, J.W., and Weindruch, R. (2009). Caloric
1100 Restriction Delays Disease Onset and Mortality in Rhesus Monkeys. Science *325*, 201-204.
1101 10.1126/science.1173635.

1102 Colman, R.J., Beasley, T.M., Kemnitz, J.W., Johnson, S.C., Weindruch, R., and Anderson, R.M.
1103 (2014). Caloric restriction reduces age-related and all-cause mortality in rhesus monkeys. Nat
1104 Commun *5*, 3557. 10.1038/ncomms4557.

1105 Colwill, R.M. (2019). Behavioral studies of stimulus learning in zebrafish larvae. Behav
1106 Processes *164*, 150-156. 10.1016/j.beproc.2019.04.005.

1107 Das, G., Klappenbach, M., Vrontou, E., Perisse, E., Clark, C.M., Burke, C.J., and Waddell, S.
1108 (2014). Drosophila learn opposing components of a compound food stimulus. Curr Biol *24*,
1109 1723-1730. 10.1016/j.cub.2014.05.078.

1110 Di Cicco, E., Tozzini, E.T., Rossi, G., and Cellerino, A. (2011). The short-lived annual fish
1111 Nothobranchius furzeri shows a typical teleost aging process reinforced by high incidence of
1112 age-dependent neoplasias. Experimental Gerontology *46*, 249-256. 10.1016/j.exger.2010.10.011.

1113 Dobin, A., Davis, C.A., Schlesinger, F., Drenkow, J., Zaleski, C., Jha, S., Batut, P., Chaisson,
1114 M., and Gingeras, T.R. (2013). STAR: ultrafast universal RNA-seq aligner. Bioinformatics *29*,
1115 15-21. 10.1093/bioinformatics/bts635.

1116 Doyle, J.M., Merovitch, N., Wyeth, R.C., Stoyek, M.R., Schmidt, M., Wilfart, F., Fine, A., and
1117 Croll, R.P. (2017). A simple automated system for appetitive conditioning of zebrafish in their
1118 home tanks. Behav Brain Res *317*, 444-452. 10.1016/j.bbr.2016.09.044.

1119 Dunn, T.W., Marshall, J.D., Severson, K.S., Aldarondo, D.E., Hildebrand, D.G.C., Chettih, S.N.,
1120 Wang, W.L., Gellis, A.J., Carlson, D.E., Aronov, D., et al. (2021). Geometric deep learning
1121 enables 3D kinematic profiling across species and environments. Nat Methods *18*, 564-573.
1122 10.1038/s41592-021-01106-6.

1123 Fard, M.S., Pasmans, F., Adriaensen, C., Laing, G.D., Janssens, G.P., and Martel, A. (2014).
1124 Chironomidae bloodworms larvae as aquatic amphibian food. Zoo Biol *33*, 221-227.
1125 10.1002/zoo.21122.

1126 Flagel, S.B., and Robinson, T.E. (2017). Neurobiological Basis of Individual Variation in
1127 Stimulus-Reward Learning. Curr Opin Behav Sci *13*, 178-185. 10.1016/j.cobeha.2016.12.004.

1128 Fontana, L., and Partridge, L. (2015). Promoting Health and Longevity through Diet: From
1129 Model Organisms to Humans. Cell *161*, 106-118. 10.1016/j.cell.2015.02.020.

1130 Genade, T., Benedetti, M., Terzibasi, E., Roncaglia, P., Valenzano, D.R., Cattaneo, A., and
1131 Cellerino, A. (2005). Annual fishes of the genus Nothobranchius as a model system for aging
1132 research. Aging Cell *4*, 223-233. 10.1111/j.1474-9726.2005.00165.x.

1133 Goodrick, C.L., Ingram, D.K., Reynolds, M.A., Freeman, J.R., and Cider, N.L. (1983).
1134 Differential effects of intermittent feeding and voluntary exercise on body weight and lifespan in
1135 adult rats. J Gerontol *38*, 36-45. 10.1093/geronj/38.1.36.

1136 Gosztolai, A., Gunel, S., Lobato-Rios, V., Pietro Abrate, M., Morales, D., Rhodin, H., Fua, P.,
1137 and Ramdya, P. (2021). LiftPose3D, a deep learning-based approach for transforming two-
1138 dimensional to three-dimensional poses in laboratory animals. Nat Methods *18*, 975-981.
1139 10.1038/s41592-021-01226-z.

1140 Green, C.L., Lamming, D.W., and Fontana, L. (2022). Molecular mechanisms of dietary
1141 restriction promoting health and longevity. Nat Rev Mol Cell Biol *23*, 56-73. 10.1038/s41580-
1142 021-00411-4.

1143 Hahn, O., Gronke, S., Stubbs, T.M., Ficz, G., Hendrich, O., Krueger, F., Andrews, S., Zhang, Q.,
1144 Wakelam, M.J., Beyer, A., et al. (2017). Dietary restriction protects from age-associated DNA
1145 methylation and induces epigenetic reprogramming of lipid metabolism. Genome Biol *18*, 56.
1146 10.1186/s13059-017-1187-1.

1147 Harel, I., Benayoun, B.A., Machado, B., Singh, P.P., Hu, C.K., Pech, M.F., Valenzano, D.R.,
1148 Zhang, E., Sharp, S.C., Artandi, S.E., and Brunet, A. (2015). A Platform for Rapid Exploration
1149 of Aging and Diseases in a Naturally Short-Lived Vertebrate. Cell *160*, 1013-1026.
1150 10.1016/j.cell.2015.01.038.

1151 Harel, I., and Brunet, A. (2015). The African Turquoise Killifish: A Model for Exploring
1152 Vertebrate Aging and Diseases in the Fast Lane. Cold Spring Harb Symp Quant Biol *80*, 275-
1153 279. 10.1101/sqb.2015.80.027524.

1154 Hartmann, N., and Englert, C. (2012). A microinjection protocol for the generation of transgenic
1155 killifish (Species: Nothobranchius furzeri). Dev Dyn *241*, 1133-1141. 10.1002/dvdy.23789.

1156 Hartmann, N., Reichwald, K., Wittig, I., Drose, S., Schmeisser, S., Luck, C., Hahn, C., Graf, M.,
1157 Gausmann, U., Terzibasi, E., et al. (2011). Mitochondrial DNA copy number and function
1158 decrease with age in the short-lived fish Nothobranchius furzeri. Aging Cell *10*, 824-831.
1159 10.1111/j.1474-9726.2011.00723.x.

1160 Honjoh, S., Ihara, A., Kajiwara, Y., Yamamoto, T., and Nishida, E. (2017). The Sexual
1161 Dimorphism of Dietary Restriction Responsiveness in Caenorhabditis elegans. Cell Rep *21*,
1162 3646-3652. 10.1016/j.celrep.2017.11.108.

1163 Houthoofd, K., and Vanfleteren, J.R. (2007). Public and private mechanisms of life extension in
1164 Caenorhabditis elegans. Molecular Genetics and Genomics *277*, 601-617. 10.1007/s00438-007-
1165 0225-1.

1166 Hu, C.K., and Brunet, A. (2018). The African turquoise killifish: A research organism to study
1167 vertebrate aging and diapause. Aging Cell *17*, UNSP e12757. 10.1111/acel.12757.

1168 Hu, C.K., Wang, W., Brind'Amour, J., Singh, P.P., Reeves, G.A., Lorincz, M.C., Alvarado, A.S.,
1169 and Brunet, A. (2020). Vertebrate diapause preserves organisms long term through Polycomb
1170 complex members. Science *367*, 870-+. 10.1126/science.aaw2601.

1171 Hunt, N.J., Kang, S.W.S., Lockwood, G.P., Le Couteur, D.G., and Cogger, V.C. (2019).
1172 Hallmarks of Aging in the Liver. Comput Struct Biotechnol J *17*, 1151-1161.
1173 10.1016/j.csbj.2019.07.021.

1174 Inness, C.L., and Metcalfe, N.B. (2008). The impact of dietary restriction, intermittent feeding
1175 and compensatory growth on reproductive investment and lifespan in a short-lived fish. Proc
1176 Biol Sci *275*, 1703-1708. 10.1098/rspb.2008.0357.

1177 Jarrard, L.E. (1993). On the role of the hippocampus in learning and memory in the rat. Behav
1178 Neural Biol *60*, 9-26. 10.1016/0163-1047(93)90664-4.

1179 Kane, A.E., Sinclair, D.A., Mitchell, J.R., and Mitchell, S.J. (2018). Sex differences in the
1180 response to dietary restriction in rodents. Curr Opin Physiol *6*, 28-34.
1181 10.1016/j.cophys.2018.03.008.

1182 Karashchuk, P., Rupp, K.L., Dickinson, E.S., Walling-Bell, S., Sanders, E., Azim, E., Brunton,
1183 B.W., and Tuthill, J.C. (2021). Anipose: A toolkit for robust markerless 3D pose estimation. Cell
1184 Rep *36*, 109730. 10.1016/j.celrep.2021.109730.

1185 Kauffman, A.L., Ashraf, J.M., Corces-Zimmerman, M.R., Landis, J.N., and Murphy, C.T.
1186 (2010). Insulin signaling and dietary restriction differentially influence the decline of learning
1187 and memory with age. PLoS Biol *8*, e1000372. 10.1371/journal.pbio.1000372.

1188 Kuhla, A., Hahn, S., Butschkau, A., Lange, S., Wree, A., and Vollmar, B. (2014). Lifelong
1189 caloric restriction reprograms hepatic fat metabolism in mice. J Gerontol A Biol Sci Med Sci *69*,
1190 915-922. 10.1093/gerona/glt160.

1191 Lange, M., Solak, A., Vijay Kumar, S., Kobayashi, H., Yang, B., and Royer, L.A. (2021). ZAF,
1192 the first open source fully automated feeder for aquatic facilities. Elife *10*. 10.7554/eLife.74234.

1193 Li, H., Handsaker, B., Wysoker, A., Fennell, T., Ruan, J., Homer, N., Marth, G., Abecasis, G.,
1194 Durbin, R., and Genome Project Data Processing, S. (2009). The Sequence Alignment/Map
1195 format and SAMtools. Bioinformatics *25*, 2078-2079. 10.1093/bioinformatics/btp352.

1196 Liao, C.Y., Rikke, B.A., Johnson, T.E., Diaz, V., and Nelson, J.F. (2010). Genetic variation in
1197 the murine lifespan response to dietary restriction: from life extension to life shortening. Aging
1198 Cell *9*, 92-95. 10.1111/j.1474-9726.2009.00533.x.

1199 Liao, Y., Smyth, G.K., and Shi, W. (2014). featureCounts: an efficient general purpose program
1200 for assigning sequence reads to genomic features. Bioinformatics *30*, 923-930.
1201 10.1093/bioinformatics/btt656.

1202 Lim, J.P., Fehlauer, H., Das, A., Saro, G., Glauser, D.A., Brunet, A., and Goodman, M.B.
1203 (2018). Loss of CaMKI Function Disrupts Salt Aversive Learning in C. elegans. J Neurosci *38*,
1204 6114-6129. 10.1523/JNEUROSCI.1611-17.2018.

1205 Longo, V.D., and Anderson, R.M. (2022). Nutrition, longevity and disease: From molecular
1206 mechanisms to interventions. Cell *185*, 1455-1470. 10.1016/j.cell.2022.04.002.

1207 Love, M.I., Huber, W., and Anders, S. (2014). Moderated estimation of fold change and
1208 dispersion for RNA-seq data with DESeq2. Genome Biol *15*, 550. 10.1186/s13059-014-0550-8.

1209 Lutter, M., and Nestler, E.J. (2009). Homeostatic and hedonic signals interact in the regulation of
1210 food intake. J Nutr *139*, 629-632. 10.3945/jn.108.097618.

1211 Maeso-Diaz, R., Ortega-Ribera, M., Fernandez-Iglesias, A., Hide, D., Munoz, L., Hessheimer,
1212 A.J., Vila, S., Frances, R., Fondevila, C., Albillos, A., et al. (2018). Effects of aging on liver
1213 microcirculatory function and sinusoidal phenotype. Aging Cell *17*, e12829. 10.1111/acel.12829.

1214 Magwere, T., Chapman, T., and Partridge, L. (2004). Sex differences in the effect of dietary
1215 restriction on life span and mortality rates in female and male Drosophila melanogaster. J
1216 Gerontol A Biol Sci Med Sci *59*, 3-9. 10.1093/gerona/59.1.b3.

1217 Mair, W., and Dillin, A. (2008). Aging and survival: the genetics of life span extension by
1218 dietary restriction. Annu Rev Biochem *77*, 727-754.
1219 10.1146/annurev.biochem.77.061206.171059.

1220 Manabe, K., Dooling, R.J., and Takaku, S. (2013). An automated device for appetitive
1221 conditioning in zebrafish (Danio rerio). Zebrafish *10*, 518-523. 10.1089/zeb.2012.0776.

1222 Mathis, A., Mamidanna, P., Cury, K.M., Abe, T., Murthy, V.N., Mathis, M.W., and Bethge, M.
1223 (2018). DeepLabCut: markerless pose estimation of user-defined body parts with deep learning.
1224 Nat Neurosci *21*, 1281-1289. 10.1038/s41593-018-0209-y.

1225 Matsui, H., Kenmochi, N., and Namikawa, K. (2019). Age- and alpha-Synuclein-Dependent
1226 Degeneration of Dopamine and Noradrenaline Neurons in the Annual Killifish Nothobranchius
1227 furzeri. Cell Rep *26*, 1727-1733 e1726. 10.1016/j.celrep.2019.01.015.

1228 Mattison, J.A., Colman, R.J., Beasley, T.M., Allison, D.B., Kemnitz, J.W., Roth, G.S., Ingram,
1229 D.K., Weindruch, R., de Cabo, R., and Anderson, R.M. (2017). Caloric restriction improves
1230 health and survival of rhesus monkeys. Nature Communications *8*, 14063.
1231 10.1038/ncomms14063.

1232 Mattison, J.A., Roth, G.S., Beasley, T.M., Tilmont, E.M., Handy, A.M., Herbert, R.L., Longo,
1233 D.L., Allison, D.B., Young, J.E., Bryant, M., et al. (2012). Impact of caloric restriction on health
1234 and survival in rhesus monkeys from the NIA study. Nature *489*, 318-321. 10.1038/nature11432.

1235 Meyer, P.J., Lovic, V., Saunders, B.T., Yager, L.M., Flagel, S.B., Morrow, J.D., and Robinson,
1236 T.E. (2012). Quantifying individual variation in the propensity to attribute incentive salience to
1237 reward cues. PLoS One *7*, e38987. 10.1371/journal.pone.0038987.

1238 Mitchell, S.J., Bernier, M., Mattison, J.A., Aon, M.A., Kaiser, T.A., Anson, R.M., Ikeno, Y.,
1239 Anderson, R.M., Ingram, D.K., and de Cabo, R. (2019). Daily Fasting Improves Health and
1240 Survival in Male Mice Independent of Diet Composition and Calories. Cell Metabolism *29*, 221-
1241 +. 10.1016/j.cmet.2018.08.011.

1242 Mitchell, S.J., Madrigal-Matute, J., Scheibye-Knudsen, M., Fang, E., Aon, M., Gonzalez-Reyes,
1243 J.A., Cortassa, S., Kaushik, S., Gonzalez-Freire, M., Patel, B., et al. (2016). Effects of Sex,
1244 Strain, and Energy Intake on Hallmarks of Aging in Mice. Cell Metab *23*, 1093-1112.
1245 10.1016/j.cmet.2016.05.027.

1246 Moore, B.C., Martinez, E., Gay, J.M., and Rice, D.H. (2003). Survival of Salmonella enterica in
1247 freshwater and sediments and transmission by the aquatic midge Chironomus tentans
1248 (Chironomidae: Diptera). Appl Environ Microbiol *69*, 4556-4560. 10.1128/AEM.69.8.4556-
1249 4560.2003.

1250 Mootha, V.K., Lindgren, C.M., Eriksson, K.F., Subramanian, A., Sihag, S., Lehar, J., Puigserver,
1251 P., Carlsson, E., Ridderstrale, M., Laurila, E., et al. (2003). PGC-1alpha-responsive genes
1252 involved in oxidative phosphorylation are coordinately downregulated in human diabetes. Nat
1253 Genet *34*, 267-273. 10.1038/ng1180.

1254 Newman, J.C., Covarrubias, A.J., Zhao, M., Yu, X., Gut, P., Ng, C.P., Huang, Y., Haldar, S., and
1255 Verdin, E. (2017). Ketogenic Diet Reduces Midlife Mortality and Improves Memory in Aging
1256 Mice. Cell Metab *26*, 547-557 e548. 10.1016/j.cmet.2017.08.004.

1257 Olton, D.S., and Samuelson, R.J. (1976). Remembrance of places passed: Spatial memory in rats.
1258 Journal of Experimental Psychology: Animal Behavior Processes *2*, 97-116. 10.1037/0097-
1259 7403.2.2.97.

1260 Partridge, L., Piper, M.D.W., and Mair, W. (2005). Dietary restriction in Drosophila.
1261 Mechanisms of Ageing and Development *126*, 938-950. 10.1016/j.mad.2005.03.023.

1262 Pereira, T.D., Shaevitz, J.W., and Murthy, M. (2020). Quantifying behavior to understand the
1263 brain. Nat Neurosci *23*, 1537-1549. 10.1038/s41593-020-00734-z.

1264 Platzer, M., and Englert, C. (2016). Nothobranchius furzeri: A Model for Aging Research and
1265 More. Trends Genet *32*, 543-552. 10.1016/j.tig.2016.06.006.

1266 Poeschla, M., and Valenzano, D.R. (2020). The turquoise killifish: a genetically tractable model
1267 for the study of aging. J Exp Biol *223*. 10.1242/jeb.209296.

1268 Polacik, M., and Reichard, M. (2010). Diet overlap among three sympatric African annual
1269 killifish species Nothobranchius spp. from Mozambique. J Fish Biol *77*, 754-768.
1270 10.1111/j.1095-8649.2010.02717.x.

1271 Pylatiuk, C., Zhao, H., Gursky, E., Reischl, M., Peravali, R., Foulkes, N., and Loosli, F. (2019).
1272 DIY Automated Feeding and Motion Recording System for the Analysis of Fish Behavior. SLAS
1273 Technol *24*, 394-398. 10.1177/2472630319841412.

1274 Reichard, M., and Polacik, M. (2019). Nothobranchius furzeri, an 'instant' fish from an
1275 ephemeral habitat. Elife *8*, e41548. 10.7554/eLife.41548.

1276 Reichwald, K., Petzold, A., Koch, P., Downie, B.R., Hartmann, N., Pietsch, S., Baumgart, M.,
1277 Chalopin, D., Felder, M., Bens, M., et al. (2015). Insights into Sex Chromosome Evolution and
1278 Aging from the Genome of a Short-Lived Fish. Cell *163*, 1527-1538. 10.1016/j.cell.2015.10.071.

1279 Roberts, M.N., Wallace, M.A., Tomilov, A.A., Zhou, Z., Marcotte, G.R., Tran, D., Perez, G.,
1280 Gutierrez-Casado, E., Koike, S., Knotts, T.A., et al. (2017). A Ketogenic Diet Extends Longevity
1281 and Healthspan in Adult Mice. Cell Metab *26*, 539-546 e535. 10.1016/j.cmet.2017.08.005.

1282 Rolls, E.T. (2006). Brain mechanisms underlying flavour and appetite. Philos Trans R Soc Lond
1283 B Biol Sci *361*, 1123-1136. 10.1098/rstb.2006.1852.

1284 Rouf, M.A., and Rigney, M.M. (1993). Bacterial Florae in Larvae of the Lake Fly Chironomus
1285 plumosus. Appl Environ Microbiol *59*, 1236-1241. 10.1128/aem.59.4.1236-1241.1993.

1286 Rudy, J.W., and Sutherland, R.J. (1989). The hippocampal formation is necessary for rats to
1287 learn and remember configural discriminations. Behav Brain Res *34*, 97-109. 10.1016/s0166-
1288 4328(89)80093-2.

1289 Sison, M., and Gerlai, R. (2010). Associative learning in zebrafish (Danio rerio) in the plus
1290 maze. Behav Brain Res *207*, 99-104. 10.1016/j.bbr.2009.09.043.

1291 Stein, G.M., and Murphy, C.T. (2014). C. elegans positive olfactory associative memory is a
1292 molecularly conserved behavioral paradigm. Neurobiol Learn Mem *115*, 86-94.
1293 10.1016/j.nlm.2014.07.011.

1294 Steinberg, E.E., Gore, F., Heifets, B.D., Taylor, M.D., Norville, Z.C., Beier, K.T., Foldy, C.,
1295 Lerner, T.N., Luo, L., Deisseroth, K., and Malenka, R.C. (2020). Amygdala-Midbrain
1296 Connections Modulate Appetitive and Aversive Learning. Neuron *106*, 1026-1043 e1029.
1297 10.1016/j.neuron.2020.03.016.

1298 Subramanian, A., Tamayo, P., Mootha, V.K., Mukherjee, S., Ebert, B.L., Gillette, M.A.,
1299 Paulovich, A., Pomeroy, S.L., Golub, T.R., Lander, E.S., and Mesirov, J.P. (2005). Gene set
1300 enrichment analysis: a knowledge-based approach for interpreting genome-wide expression
1301 profiles. Proc Natl Acad Sci U S A *102*, 15545-15550. 10.1073/pnas.0506580102.

1302 Swindell, W.R. (2008). Comparative analysis of microarray data identifies common responses to
1303 caloric restriction among mouse tissues. Mech Ageing Dev *129*, 138-153.
1304 10.1016/j.mad.2007.11.003.

1305 Swindell, W.R. (2009). Genes and gene expression modules associated with caloric restriction
1306 and aging in the laboratory mouse. BMC Genomics *10*, 585. 10.1186/1471-2164-10-585.

1307 Swindell, W.R. (2012). Dietary restriction in rats and mice: a meta-analysis and review of the
1308 evidence for genotype-dependent effects on lifespan. Ageing Res Rev *11*, 254-270.
1309 10.1016/j.arr.2011.12.006.

1310 Terzibasi, E., Lefrancois, C., Domenici, P., Hartmann, N., Graf, M., and Cellerino, A. (2009).
1311 Effects of dietary restriction on mortality and age-related phenotypes in the short-lived fish
1312 Nothobranchius furzeri. Aging Cell *8*, 88-99. 10.1111/j.1474-9726.2009.00455.x.

1313 Terzibasi, E., Valenzano, D.R., Benedetti, M., Roncaglia, P., Cattaneo, A., Domenici, L., and
1314 Cellerino, A. (2008). Large Differences in Aging Phenotype between Strains of the Short-Lived
1315 Annual Fish Nothobranchius furzeri. Plos One *3*, e3866. 10.1371/journal.pone.0003866.

1316 Turturro, A., Witt, W.W., Lewis, S., Hass, B.S., Lipman, R.D., and Hart, R.W. (1999). Growth
1317 curves and survival characteristics of the animals used in the Biomarkers of Aging Program. J
1318 Gerontol A Biol Sci Med Sci *54*, B492-501. 10.1093/gerona/54.11.b492.

1319 Valenzano, D.R., Benayoun, B.A., Singh, P.P., Zhang, E., Etter, P.D., Hu, C.K., Clement-Ziza,
1320 M., Willemsen, D., Cui, R., Harel, I., et al. (2015). The African Turquoise Killifish Genome
1321 Provides Insights into Evolution and Genetic Architecture of Lifespan. Cell *163*, 1539-1554.
1322 10.1016/j.cell.2015.11.008.

1323 Valenzano, D.R., Kirschner, J., Kamber, R.A., Zhang, E., Weber, D., Cellerino, A., Englert, C.,
1324 Platzer, M., Reichwald, K., and Brunet, A. (2009). Mapping loci associated with tail color and

sex determination in the short-lived fish Nothobranchius furzeri. Genetics *183*, 1385-1395. 10.1534/genetics.109.108670.

Valenzano, D.R., Sharp, S., and Brunet, A. (2011). Transposon-Mediated Transgenesis in the Short-Lived African Killifish Nothobranchius furzeri, a Vertebrate Model for Aging. G3 (Bethesda) *1*, 531-538. 10.1534/g3.111.001271.

Valenzano, D.R., Terzibasi, E., Cattaneo, A., Domenici, L., and Cellerino, A. (2006a). Temperature affects longevity and age-related locomotor and cognitive decay in the short-lived fish Nothobranchius furzeri. Aging Cell *5*, 275-278. 10.1111/j.1474-9726.2006.00212.x.

Valenzano, D.R., Terzibasi, E., Genade, T., Cattaneo, A., Domenici, L., and Cellerino, A. (2006b). Resveratrol prolongs lifespan and retards the onset of age-related markers in a short-lived vertebrate. Current Biology *16*, 296-300. 10.1016/j.cub.2005.12.038.

Wang, W., Hu, C.K., Zeng, A., Alegre, D., Hu, D., Gotting, K., Ortega Granillo, A., Wang, Y., Robb, S., Schnittker, R., et al. (2020). Changes in regeneration-responsive enhancers shape regenerative capacities in vertebrates. Science *369*. 10.1126/science.aaz3090.

Weindruch, R., Walford, R.L., Fligiel, S., and Guthrie, D. (1986). The retardation of aging in mice by dietary restriction: longevity, cancer, immunity and lifetime energy intake. J Nutr *116*, 641-654. 10.1093/jn/116.4.641.

Wendler, S., Hartmann, N., Hoppe, B., and Englert, C. (2015). Age-dependent decline in fin regenerative capacity in the short-lived fish Nothobranchius furzeri. Aging Cell *14*, 857-866. 10.1111/acel.12367.

Yang, P., Yamaki, M., Kuwabara, S., Kajiwara, R., and Itoh, M. (2019). A newly developed feeder and oxygen measurement system reveals the effects of aging and obesity on the metabolic rate of zebrafish. Exp Gerontol *127*, 110720. 10.1016/j.exger.2019.110720.

Ye, J., and Medzhitov, R. (2019). Control strategies in systemic metabolism. Nat Metab *1*, 947-957. 10.1038/s42255-019-0118-8.

Yu, G., Wang, L.G., Han, Y., and He, Q.Y. (2012). clusterProfiler: an R package for comparing biological themes among gene clusters. OMICS *16*, 284-287. 10.1089/omi.2011.0118.

Zak, J., Dykova, I., and Reichard, M. (2020). Good performance of turquoise killifish (Nothobranchius furzeri) on pelleted diet as a step towards husbandry standardization. Sci Rep *10*, 8986. 10.1038/s41598-020-65930-0.

Zak, J., and Reichard, M. (2021). Reproductive senescence in a short-lived fish. J Anim Ecol *90*, 492-502. 10.1111/1365-2656.13382.

1357 Zak, J., Roy, K., Dykova, I., Mraz, J., and Reichard, M. (2022). Starter feed for carnivorous
1358 species as a practical replacement of bloodworms for a vertebrate model organism in ageing, the
1359 turquoise killifish Nothobranchius furzeri. J Fish Biol *100*, 894-908. 10.1111/jfb.15021.

1360 Zupkovitz, G., Lagger, S., Martin, D., Steiner, M., Hagelkruys, A., Seiser, C., Schofer, C., and
1361 Pusch, O. (2018). Histone deacetylase 1 expression is inversely correlated with age in the short-
1362 lived fish Nothobranchius furzeri. Histochemistry and Cell Biology *150*, 255-269.
1363 10.1007/s00418-018-1687-4.
1364

Table 1: Automated feeding allows for more flexible, frequent, and precise feedings than manual feeding. Manual feeding is restricted to the times of the day when researchers can enter the animal facilities based on day/night cycles, whereas automated feeding can be programmed to occur at any time of the day or night. Manual feeding is restricted by the researcher's ability to feed, while automated feeding can occur as frequently as 144 times per day. Manual feeding requires individual attention to each tank on a daily basis, multiple times per day, whereas automated feeding requires an initial setup and biweekly checks to replace batteries and add food to the devices. Manual feeding is relatively imprecise at 0.016 (the inverse of the variance of food delivered), while automated feeding has a higher precision at 0.512.

	Manual feeding	Automated feeding
Schedule flexibility	Limited to weekday working hours	24/7
Maximum frequency	2-3 times a day	144 times a day
Labor required	Daily, linearly increasing with tanks	Initial setup and biweekly checks
Precision	Low, with batch effects for different individuals (0.016)	Higher (0.512)

Figure 1: An automated 3D-printed feeding system for the African turquoise killifish
(A) Side view of an individual automated feeding unit placed on the top front of a 2.8 L fish tank supplied by Aquaneering™. Dark arrowhead: feeding unit on the lid of a tank.
(B) Top view of an individual automated feeding unit. This is a compact, self-contained unit with individual power supply, food hopper, stepper motor for food delivery, and microcontroller for control and communication. White arrowhead: hopper where the dry food is placed.
(C) Components of an individual automated feeder. Each feeder is composed of a lithium ion battery and holder (a), 3D printed parts (b) coupled with a custom printed circuit board (c), a Wemos D1 mini ESP8266-based microcontroller board (d), laser cut acrylic parts (e), and stepper motor (f).
(D) Users control the automated feeding system by interacting with a cloud-based server. This server communicates with small local servers on the premise, which then communicate with the individual automated feeders. Changes to feeding schedules are provided by users and filter down to the appropriate feeders, while status updates, such as feeding confirmations, make the return trip back to the users.

Figure 2: Fidelity and precision of the automated feeding system

(A) Logged feedings per day from a representative feeder over a 30-day period, with 7 feedings of 5 mg programmed for each day. Note that a recording of six feedings instead of seven does not necessarily mean that the feeding was missed but could be due to an unlogged feeding due to inability to connect to main server. Source data: Figure 2-Source Data 1

(B-C) Histogram (B) of deviations from scheduled feedings for 2279 days of feedings over 41 feeders with a given number of deviations tabulated in (C). The vast majority (>98%) of feedings have 0 or 1 missed feeding. Source data: Figure 2-Source Data 2

(D) Automated feeding provides higher feeding precision than manual feeding as seen from the dispersion of feeding volumes as a percentage of the mean. When compared to manual feeding by multiple individual users or a single individual, automated feeders are more precise in the amount of food delivered. Precision is defined as the reciprocal of the estimated variance given either six individuals (n = 54, precision = 0.016), one individual (n = 9, precision = 0.082), four feeders (n = 19, precision = 0.512), or one single feeder (n = 10, precision = 0.559). Precision derived from bootstrapped estimates of the standard deviation for each group. Source data: Figure 2-Source Data 3.

Figure 3: Automated feeding enables the definition of different diets for the African killifish
(A) Experimental scheme to compare two automated feeding schedules for killifish: feeding 7 times a day evenly over 12 hours (5 mg Otohime fish diet per feeding, 35 mg total per day) and feeding 3 times a day within a 2-hour period in the morning (5 mg Otohime fish diet per feeding, 15 mg total per day). These regimens were applied from 1 month of age to death (for growth measurements) and from 1 month of age until death of one individual in the pair (for fertility measurements). For fertility measurements, each individual in the pair was fed individually while single-housed and then crossed for 24 hours once per week to assess fertility.
(B) The average growth rate (cm/week) of male killifish from 1 month of age to death fed either 7 times a day (blue, median = 0.3726 cm/week, n = 8) is significantly greater than those fed 3 times a day in the morning (orange, median = 0.3 cm/week, n = 3). Each dot represents a single animal's growth averaged over its lifespan. Animals that lived longer than 4 months were not considered due to concerns with non-linear growth rate. Significance determined by Wilcoxon rank sum test ($p = 0.012$). Animals were from the same cohort as Figure 4-figure supplement 1 (cohort 1). Source data: Figure 3-Source Data 1.
(C) The average growth rate (cm/week) of female killifish from 1 month of age to death fed 7 times a day (blue, median = 0.3461 cm/week, n = 9) is significantly greater than those fed 3 times a day in the morning (orange, median = 0.2690 cm/week, n = 8). Each dot represents a single animal's growth averaged over their lifespan. Animals that lived longer than 4 months were not considered due to concerns with non-linear growth rate. Significance determined by Wilcoxon rank sum test ($p = 0.060$). Animals were from the same cohort as Figure 4-figure supplement 1 (cohort 1). Source data: Figure 3-Source Data 1.
(D) Killifish mating pairs (one male and one female) fed 3 times a day are significantly less fertile (median = 1 fertilized embryo per mating, n = 30 matings across 5 pairs) than mating pairs fed 7 times a day (median = 4 fertilized embryos per mating, n = 30 matings across 5 pairs). Each dot represents the fertilized embryos collected from one pair crossing overnight, and pairs were mated from 8 weeks of age until one individual in the pair died. Significance determined by Wilcoxon rank sum test ($p = 0.0005$). Source data: Figure 3-Source Data 2 and 3.
(E) Experimental scheme to compare two automated feeding schedules for killifish: feeding 12 times a day (5 mg Otohime fish diet per feeding, 60 mg total per day) compared to feeding 7 times a day (5 mg Otohime fish diet per feeding, 35 mg total per day). These regimens were applied from 1 month of age to death (for growth measurements) and from 2 months of age until death of one individual in the pair (for fertility measurements). For fertility measurements, each individual in the pair was fed individually while single-housed and then crossed for 24 hours once per week to assess fertility.
(F) The average growth rate (cm/week) of male killifish from 1 month of age to death is significantly higher for animals fed 12 times a day (black, median = 0.4917 cm/week, n = 13 males) than for animals fed 7 times a day (blue, median = 0.4092 cm/week, n = 5 males). Each dot represents a single animal's growth averaged over its lifespan. Animals that lived longer than 4 months were not considered due to concerns with non-linear growth rate. Significance determined by Wilcoxon rank sum test ($p = 0.0068$). Source data: Figure 3-Source Data 4.
(G) The average growth rate (cm/week) of female killifish from 1 month of age to death is significantly higher for animals fed 12 times a day (black, median = 0.4268 cm/week, n = 9

females) than for animals fed 7 times a day (blue, median = 0.3425 cm/week, n = 11 females). Each dot represents a single animal's growth averaged over its lifespan. Animals that lived longer than 4 months were not considered due to concerns with non-linear growth rate. Significance determined by Wilcoxon rank sum test (p = 0.012). Source data: Figure 3-Source Data 4.
(H) Killifish mating pair fertility is significantly lower for animals fed 12 times a day (black feeding schedule, median = 5 fertilized embryos per mating, n = 23 matings) than for animals fed 7 times a day (blue feeding schedule, median = 11 fertilized embryos per mating, n = 21 matings). Each dot represents fertilized embryos collected from one pair upon crossing for 24 hours and pairs were mated from 2 months of age until one individual in the pair died. Significance determined by Wilcoxon rank sum test (p = 0.017). Source data: Figure 3-Source Data 5 and 6.

Figure 4: An amount and time-restricted dietary regimen robustly extends lifespan in male, but not female African turquoise killifish

(A) Experimental scheme comparing two automated feeding schedules for killifish: an *ad libitum* (AL) regimen (7 times a day, 35 mg Otohime fish diet per day, blue) or a dietary restricted (DR) regimen (3 times in the morning, 15 mg Otohime fish diet per day, orange). Automated feeding regimens were started after sexual maturity, at 1 month of age.

(B) Male killifish fed a dietary restricted regimen (solid orange, median lifespan = 116 days, n = 21) lived significantly longer than male killifish fed an *ad libitum* regimen (solid blue, median lifespan = 95 days, n = 21) (p = 0.0031, logrank test). Source data: Figure 4-Source Data 1.

(C) Female killifish fed a dietary restricted regimen (dashed orange, median lifespan = 90 days, n = 25) did not live significantly longer than female killifish fed an *ad libitum* regimen (dashed blue, median lifespan = 82.5 days, n = 24) (p = 0.6798, logrank test). Source data: Figure 4-Source Data 1.

(D) In *ad libitum* conditions, male killifish (solid blue, median lifespan = 95 days, n = 21) did not exhibit lifespan difference from female killifish (dashed blue, median lifespan = 82.5 days, n = 24) (p = 0.3282, logrank test). Source data: Figure 4-Source Data 1.

(E) In dietary restricted conditions, male killifish (solid orange, median lifespan = 116 days, n = 21) lived significantly longer than female killifish (dashed orange, median lifespan = 90 days, n = 25) (p = 0.0005, logrank test). Source data: Figure 4-Source Data 1.

(F) Fitted curve of the binned 27-day hazard rate of male killifish from both cohorts to a Gompertz distribution and then transformed into the natural log of the hazard rate. The estimated "rate of aging" (slope) of killifish on the AL feeding regimen is 0.3388 (95% confidence interval = 0.2437 to 0.434) and is significantly different from the rate of aging for DR, which is 0.1457 (95% confidence interval = 0.0846 to 0.2069). The estimated "frailty" (intercept) for killifish on the AL feeding regimen is 0.0385 (95% confidence interval = 0.0203 to 0.073) compared to 0.0557 (95% confidence interval = 0.0315 to 0.0986) for killifish on DR (overlapping confidence intervals for intercept parameter indicate that these parameters are not significant). Source data: Figure 4-Source Data 1 and 2.

Figure 5: Transcriptomic analysis shows that an amount- and time-restricted DR induces sex-specific gene expression in the liver of the killifish

(A) Experimental scheme to compare the liver and brain transcriptomes in *ad libitum* (AL) or dietary restriction (DR) conditions, for males and females. A 5-week amount- and time-restricted DR regimen was used (similar to Figure 4) and 4 animals per sex (n = 4) were used.

(B) Principal component analysis (PCA) of the transcriptomes of all liver samples (PC1 and PC3), or brain samples (PC1 and PC2), with samples coded by sex and diet regimens. For other PCs, see Figure 5-figure supplement 1A, B. Variance stabilization transformation was applied to the raw counts, and the transformed count data were used as PCA input. Each symbol represents the full transcriptome of one individual fish.

(C) Selected GSEA results, comparing the AL and DR transcriptomes for males and females. Dot color represents the normalized enrichment score of each GO term. Red, higher expression in DR; blue, lower expression in DR. Dot size represents the –log10 of the adjusted P-value (i.e., false discovery rate (FDR) after multiple hypotheses testing).

(D) Average scaled expression of the genes underlying specific GO terms. The average scaled expression of the 4 replicates per condition (Female AL; Female DR, Male AL; Male DR) was plotted in the heatmaps (see Materials and Methods). Red, higher expression in DR; blue, lower in DR.

(E) Sex DEGs (identified in AL) were enriched in diet DEGs, for both males and females. The non-diet DEGs control gene set ("control") and the diet DEGs shared the same transcript expression distribution and gene group size (see Materials and Methods). The percentage of genes being sex DEGs for each gene set ("enrichment") was plotted as pie-charts. The number of genes in each gene set (n) is indicated in parentheses. Significance determined by a 2-tailed Fisher's exact test. For the control gene sets, the median p-value and enrichment in the bootstrapped results were reported.

Figure 6: Use of automated feeder for assessing positive associative learning behavior

(A) Schematic for the killifish positive associative behavior assay. The red light switches on at 2 seconds after the video recording starts, and the food is dropped at the water surface 7 seconds later (so 9 seconds after the recording starts). Unsuccessful association occurs when the killifish does not initiate a surface-bound trajectory within the 7-second window, between the light turning on and the food dropping (so between 2 and 9 seconds after the recording starts) (top row). Successful association occurs when the killifish initiates a surface-bound trajectory within this 7-second window (bottom row).

(B) Schematic for the automated analysis pipeline. The head and tail positions of the fish and the location of where food was dropped were annotated for selected frames and used to train the DeepLabCut network. After processing all the videos on the trained settings, the results were filtered based on likelihood, anomalous frames were identified and removed, and splines interpolation was performed (see Materials and Methods). The resulting head positions of the fish were used for velocity and trajectory calculations.

(C) Recording video frames from the front of the 2.8 L tank. Top row, an example trial (Trial 4) of Fish 3, where this fish was unsuccessful in associating food with the red light. Bottom row, an example trial (Trial 17) where this fish was successful in associating food with light by moving toward the water surface after the red light turns on and before food is dropped. White arrow points to the fish's position.

(D) Trajectory traces generated by the automated pipeline for the videos in (C). The x-positions (along the tank width) and y-positions (along the tank height) of Fish 3 are tracked at each video frame from 2 seconds after the recording started to 9 seconds, and colored according to time. The food drop site indicates where the food arrives at the water surface, and the red light, where the LED light is located. Trial 4, a trial of unsuccessful association; Trial 17, a trial of successful association.

(E) The vertical component (y-component) of the fish's (Fish 3) velocity, graphed as a heatmap across trial number. The rolling average of 20 frames is plotted for each second of each trial. When the fish exhibits a fast trajectory toward the surface, the pixels/second value is higher (more yellow); whereas when the fish exhibits a slow trajectory toward the surface (or away from surface), the pixels/second value is smaller (bluer). Asterisks indicate successful trials.

(F) The initiation time of the first surface-bound trajectory (t_1) across trials for all fish, quantified by the automated pipeline. Each fish went through 17 trials. The mean t_1 for all the fish was calculated for each trial (n = 13), then plotted as a function of trial numbers. A trial was considered successful if t_1 was between 2 and 9 seconds (inclusive). Error bars represent one standard deviation above and below the mean t_1.

(G) The average t_1 of the first 7 trials vs. the last 7 trials for each fish, quantified by the automated pipeline. Each symbol represents the average t_1 for one fish, and the same symbol denotes the same fish. Males, closed symbols; females, open symbols. Significance determined by a two-tailed Wilcoxon matched-pairs signed rank test, where the average t_1 from the first and last 7 trials of the same fish is a matched pair.

(H) The percentage of successful trials for the first 7 trials vs. the last 7 trials of each fish, quantified by the automated pipeline. The symbols' shape and color, and the statistics are the same as in (G).

(I) The initiation time of the first surface-bound movement (t_1) across trials for young vs. old fish, quantified by the automated pipeline and graphed as in (F). Young, blue; old, red.
(J) The average t_1 of the first 7 trials vs. the last 7 trials, for young (blue) or old (red) fish, quantified by the automated pipeline. Males, closed symbols; females, open symbols. Statistics are the same as in (G).
(K) The percentage of successful trials for the first 7 trials vs. the last 7 trials, for young (blue) or old (red) fish, quantified by the automated pipeline. Males, closed symbols; females, open symbols. Statistics are the same as in (G).
(L) Learning index for young (blue) and old (red) killifish, quantified by the automated pipeline. The learning index is defined as the inverse of the first trial number for an animal to achieve two consecutive successes. Males, closed symbols; females, open symbols. Significance determined using a two-tailed Wilcoxon rank sum test.
(M) Learning index plotted as a function of the fish's age, quantified by the automated pipeline. Males, closed symbols; females, open symbols. R, Pearson correlation coefficient.

Figure 1-figure supplement 1: Automated feeders are designed to confirm each feeding and can be programmed to perform independent feeding regimens.

(A) Schematic showing how the automated feeder operates. Step 1, at the programmed feeding time, the feeder wakes up from idle and receives the operation instruction from the network. The 3-mm hole turns toward the hopper. Step 2, the 3-mm hole collects 5 mg of dry food from the hopper. Step 3, the 3-mm hole sits on top of the photoresistor. Because the food blocks the green LED light from reaching the photoresistor, a high value of photoresistance is recorded on the network. Step 4, the 3-mm hole carries the food toward the food drop site. Step 5, the 3-mm hole arrives at the food drop site and drops food. Then it returns to the photoresistor. Step 6, after food drops, the green LED light is no longer blocked, and a low value of photoresistance is recorded on the network. Then the 3-mm hole moves back to the resting position until next feeding. The change in photoresistance between Step 3 and 6 indicates that the food has been dropped.

(B) Schematic showing that each feeder can be programmed with separate and independent feeding regimens. Each feeder has a unique ID (associated with each Wemos D1 mini ESP8266-based development board), along with an individual set of instructions stored on the server that can be updated independently of every other feeder. This setup allows different feeding regimens to be implemented simultaneously for different tanks.

Figure 2-figure supplement 1: Fidelity and precision of the automated feeding system validated by independent researcher.

(A) Histogram of deviations from scheduled feedings for 9284 days of feedings over 90 feeders. The vast majority (>94%) of feedings have 0 or 1 missed feeding. Source data: Figure 2-Source Data 4.

(B) Deviations from scheduled feedings for 9284 days of feedings over 90 feeders with a given number of deviations tabulated. Source data: Figure 2-Source Data 4.

Figure 3-figure supplement 1: Total number of embryos produced in response to different diets

(A) Experimental scheme to compare two automated feeding schedules for killifish: feeding 7 times a day evenly over 12 hours (5 mg Otohime fish diet per feeding, 35 mg total per day) and feeding 3 times a day within a 2-hour period in the morning (5 mg Otohime fish diet per feeding, 15 mg total per day). These regimens were applied from 1 month of age until death of one individual in the pair. Each individual in the pair was fed individually while single-housed and then crossed for 24 hours once per week to assess number of embryos produced.

(B) Killifish mating pairs fed 3 times a day produce significantly fewer total embryos (median = 3 fertilized embryo per mating, n = 30 matings across 5 pairs) than mating pairs fed 7 times a day (median = 10.5 fertilized embryos per mating, n = 30 matings across 5 pairs). Each dot represents the total embryos collected from one pair crossing overnight. Significance determined by Wilcoxon rank sum test ($p = 0.0004$). Source data: Figure 3-Source Data 2 and 3.

(C) Experimental scheme to compare two automated feeding schedules for killifish: feeding 12 times a day (5 mg Otohime fish diet per feeding, 60 mg total per day) compared to feeding 7 times a day (5 mg Otohime fish diet per feeding, 35 mg total per day). These regimens were applied from 2 months of age until death of one individual in the pair. Each individual in the pair was fed individually while single-housed and then crossed for 24 hours once per week to assess the number of embryos produced.

(D) Killifish mating pairs fed 12 times a day do not produce significantly fewer total embryos (black feeding schedule, median = 12 total embryos per mating, n = 23 matings, across 3 pairs) than for those fed 7 times a day (blue feeding schedule, median = 19 total embryos per mating, n = 21 matings across 3 pairs). Each dot represents the total embryos collected from one pair crossing overnight. Significance determined by Wilcoxon rank sum test ($p = 0.15$). Source data: Figure 3-Source Data 5 and 6.

Figure 4-figure supplement 1: An independent cohort of African turquoise killifish undergoing the amount- and time-restricted dietary regimen also exhibits lifespan extension in males

(A) Experimental scheme comparing two automated feeding schedules for killifish: an *ad libitum* (AL) regimen (7 times a day, 35 mg Otohime fish diet per day, blue) or a dietary restricted (DR) regimen (3 times in the morning, 15 mg Otohime fish diet per day, orange). Feeding was started after sexual maturity, at 1 month of age.

(B) In an independent cohort (cohort 1), male killifish fed a dietary restricted regimen (solid orange, median lifespan = 142.5 days, n = 14) did not live significantly longer than male killifish fed an *ad libitum* regimen (solid blue, median lifespan = 125.5 days, n = 18) (p = 0.2373, logrank test). Source data: Figure 4-Source Data 2.

(C) In an independent cohort (cohort 1), female killifish fed an amount- and time-restricted dietary regimen (dashed orange, median lifespan = 104 days, n = 14) did not live significantly longer than female killifish fed an *ad libitum* regimen (dashed blue, median lifespan = 104 days, n = 12) (p = 0.3954, logrank test). Source data: Figure 4-Source Data 2.

(D) In an independent cohort (cohort 1) with *ad libitum* conditions, male killifish (solid blue, median lifespan = 125.5 days, n = 18) did exhibit a lifespan difference from female killifish (dashed blue, median lifespan = 104 days, n = 12) (p = 0.0299, logrank test). Source data: Figure 4-Source Data 2.

(E) In an independent cohort (cohort 1) with dietary restricted conditions, male killifish (solid orange, median lifespan = 142.5 days, n = 14) lived significantly longer than female killifish (dashed orange, median lifespan = 104 days, n = 14) (p = 0.0054, logrank test). Source data: Figure 4-Source Data 2.

(F) Combining the lifespans of the first and second cohorts of male killifish, we found the additional animals did not change the conclusion from the second cohort that male killifish on an *ad libitum* diet (solid blue, median lifespan = 106 days, n = 39) live significantly shorter than dietary restriction animals (dashed orange, median lifespan = 129 days, n = 35) (p = 0.0052, logrank test). Source data: Figure 4-Source Data 1 and 2.

Figure 5-figure supplement 1: Transcriptomic analysis shows sex-specific gene expression in response to DR in killifish livers.

(A) PCA of the liver samples in PC1 and PC2, coded by sex and diet regimens. AL, *ad libitum*; DR, amount- and time-restricted dietary restriction. Four animals per sex (n = 4) were used.

(B) PCA of the brain samples in PC1 and PC3, coded by sex and diet regimens. Four animals per sex (n = 4) were used, except one female AL sample was an outlier and excluded (see Materials and Methods).

(C) Liver transcriptomes plotted as the log10-transformed mean normalized counts and the log2 fold change (MA plots). Top left is the MA plot for females (top right, for males), comparing the liver transcriptomes between under AL and under DR. A positive log2 fold change indicates higher expression in DR. The mean of normalized counts was calculated by averaging the normalized counts across all samples. Bottom left, MA plot comparing liver transcriptomes between males and females in the *ad libitum* (AL) condition; bottom right, MA plot comparing liver transcriptomes between males and females in the amount- and time-restricted DR conditions. A positive log2 fold change indicates higher expression in males.

(D) Hypergeometric GO enrichment for the genes upregulated or downregulated in female DR liver transcriptomes, or male DR liver transcriptomes. Dot color represents the enrichment score of each GO term, with red indicating upregulation in DR and blue, downregulation in DR. Dot size, –log10 of the adjusted P-value (i.e., false discovery rate (FDR) after multiple hypotheses testing).

(E) Sex DEGs (identified in DR) were enriched in diet DEGs, for both males and females. The pie-charts were generated as in Figure 5E.

Figure 6-figure supplement 1: Use of automated feeder for assessing positive associative learning behavior

(A) Compass plots for the first 7 trials or last 7 trials, representing the frequency distribution of the angles of movement, for all fish, between the light turning on (at 2 seconds) and the food dropping (at 9 seconds). For each fish, the initial position (at 2 seconds) and the final position (at 9 seconds) were converted from Cartesian coordinates (x, y) to polar coordinates (r, θ), and the angular coordinate (θ) of the vector (from the initial position to the final position) was converted from radians to degrees. The angular coordinates (θ) from all the fish from multiple trials (the first 7 trials or the last 7 trials) were binned (bin size = 20°). The frequency distribution (histograms centered on midpoint of bin) is plotted. An angular coordinate of 90º would indicate that the average movement of the fish between 2 and 9 seconds was directly to the surface. Each "wedge" on the compass plot represents a bin. The wedge is directed toward the angle (out of 360º) that represents the midpoint of the bin and has a radius that indicates the frequency of angles in the bin (larger radius indicating that more velocity vectors fallen into that bin). All the bins have the same origin.

(B) Schematic for the manual analysis pipeline. Top, schematic for quantification metrics. For each trial, the fish position and movement were tracked second by second. If the fish displays any positive y-axis displacement (tracked by the mid-point of the fish) at a given second, then a score of "1" would be given to metric 1 ("upward movement"). If the fish is located within ~0.5 cm from the water surface, then a score of "1" would be given to metric 2 ("at surface"). Middle, occurrence of positive y-displacement; bottom, presence of the fish at the water surface, across the 18 seconds for Trial 17 of Fish 3. Light turns at 2 seconds after the video recording starts, and the food drops at the water surface at 9 seconds. The initiation time of the first surface-bound trajectory (t_1) is at 3 seconds, which is between 2-9 seconds. Thus, this trial is considered "successful."

(C) The initiation time of the first surface-bound trajectory (t_1) across trials for all fish, quantified manually. The mean t_1 and error bars are plotted as in Figure 6F.

(D) The average t_1 for the first 7 trials vs. the last 7 trials, quantified manually. The symbols' shape and color, and the statistics are the same as in Figure 6G.

(E) The percentage of successful trials for the first 7 trials vs. the last 7 trials, quantified manually. The symbols' shape and color, and the statistics are the same as in Figure 6G.

(F) Correlation of t_1 between the automated and manual pipelines. Each point represents a trial, with t_1 quantified manually ("manual t_1") or using the automated pipeline ("automated t"). A total of 219 trials were quantified, with all the trials from the 13 fish pooled. R, Pearson correlation.

(G) The average velocities for young and old fish, quantified by the automatic pipeline. For each fish, the 20-frame rolling average velocities were averaged across all frames and all trials. Each dot represents the trial average of one fish. Males, closed symbols; females, open symbols. Significance determined by Wilcoxon rank sum test.

Supplementary Material Legends

Supplemental Videos

Figure 1-video 1. Example of automatic feeder function.

Figure 6-video 1. Example of a trial with a "successful" association (Trial 17, Fish 3).

Figure 6-video 2. Example of a trial with an "unsuccessful" association (Trial 4, Fish 3).

Source Data files

Figure 1-Source Data 1. Automatic feeder parts list.

Figure 2-Source Data 1. Feeding logs from a representative feeder over a 30-day period.

Figure 2-Source Data 2. Missed feedings for 41 feeders over 2,279 days of feeding.

Figure 2-Source Data 3. Feeding data for automatic and manual feedings.

Figure 2-Source Data 4. Missed feedings for 90 feeders over 9,284 days of feeding.

Figure 3-Source Data 1. Metadata table for growth rate comparisons for males and female killifish on DR diet regimens.

Figure 3-Source Data 2. Embryo viability data for mate pairs on DR or AL diet regimens.

Figure 3-Source Data 3. Metadata table for mate pairs used in embryo viability experiments in Figure 3-Source Data 2.

Figure 3-Source Data 4. Metadata table for growth rate comparisons for males and female killifish on OE diet regimens.

Figure 3-Source Data 5. Embryo viability data for mate pairs on overfeeding or AL diet regimens.

Figure 3-Source Data 6. Metadata table for mate pairs used in embryo viability experiments in Figure 3-Source Data 5.

Figure 4-Source Data 1. Lifespan data for male and female killifish on AL and DR diet regimens (cohort 2).

Figure 4-Source Data 2. Lifespan data for male and female killifish on AL and DR diet regimens from independent cohort (cohort 1).

Figure 4-Source Data 3. Result from proportional hazards model that shows DR independently and significantly reduces the hazard rate.

Figure 5-Source Data 1. Experimental metadata for bulk RNA sequencing experiments.

Figure 5-Source Data 2. Diet DEG list (DR vs AL) for female liver tissues.

Figure 5-Source Data 3. Diet DEG list (DR vs AL) for male liver tissues.

Figure 5-Source Data 4. Sex DEG list (male vs female) for all AL liver tissues.

Figure 5-Source Data 5. Sex DEG list (male vs female) for all DR liver tissues.

Figure 5-Source Data 6. GSEA results for female diet DEGs.

Figure 5-Source Data 7. GSEA results for male diet DEGs.

Figure 5-Source Data 8. Gene ontology enrichment results for diet DEGs.

Figure 5-Source Data 9. Gene ontology enrichment results for sex DEGs.

Figure 5-Source Data 10. Diet-sex interaction DEG list.

Figure 5-Source Data 11. Bootstrap data for the control sex DEGs enrichment in diet DEGs.

Figure 6-Source Data 1. Experimental metadata for behavior experiments.

Figure 6-Source Data 2. Unfiltered raw trajectory data output from DeepLabCut.

Figure 6-Source Data 3. Filtered and interpolated trajectory data with velocity calculations.

Figure 6-Source Data 4. Initiation of upward trajectory value (t1) summary for automatic quantification.

Figure 6-Source Data 5. Fish angular coordinate data for compass plots.

Figure 6-Source Data 6. Initiation of upward trajectory value (t1) summary for manual quantification.

Figure 6-Source Data 7. Manual quantification of behavior for female killifish.

Figure 6-Source Data 8. Manual quantification of behavior for male killifish.

Figure 1

A Automated feeder (Side view)

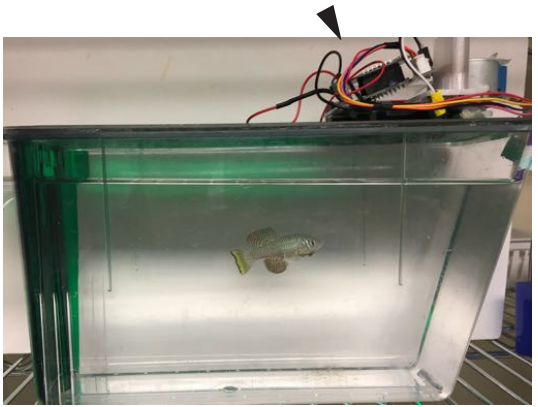

B Automated feeder (Top view)

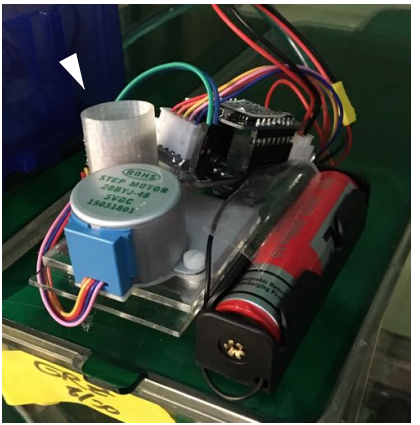

C Automated feeder hardware

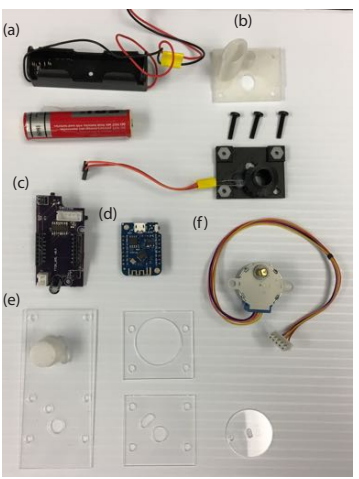

D Software schematic of information flow

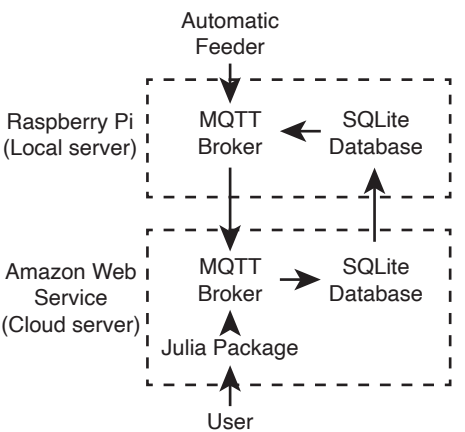

Figure 2

A Fidelity of one automated feeder

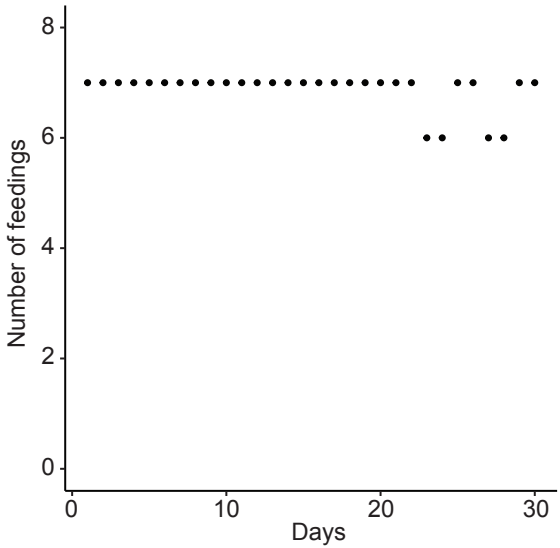

B Fidelity of multiple automated feeders

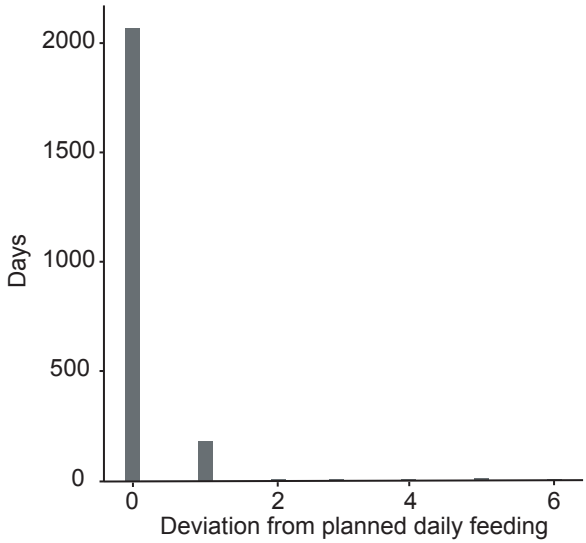

C Feeding number and frequency

Deviation from planned daily feeding	Days	Frequency
0	2069	90.79%
1	180	7.90%
2	5	0.22%
3	6	0.26%
4	4	0.18%
5	10	0.44%
6	5	0.22%

D Precision comparison between automated and manual feeding

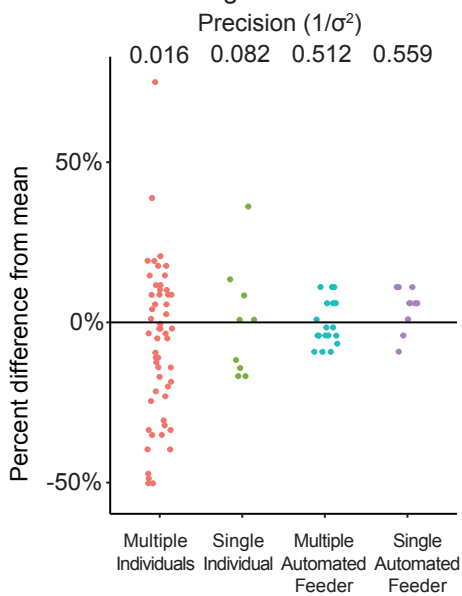

Figure 3

A Experimental scheme for dietary restriction

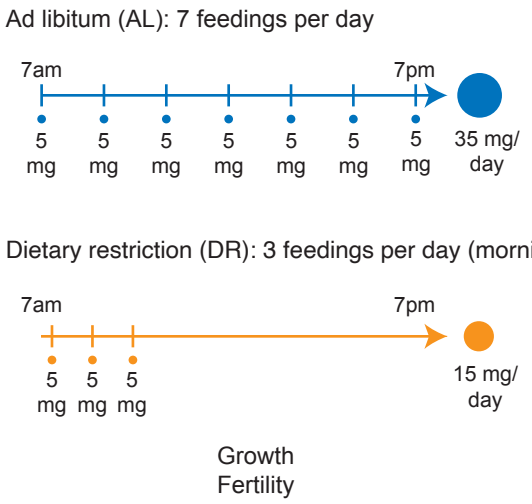

B Male growth rate upon dietary restriction

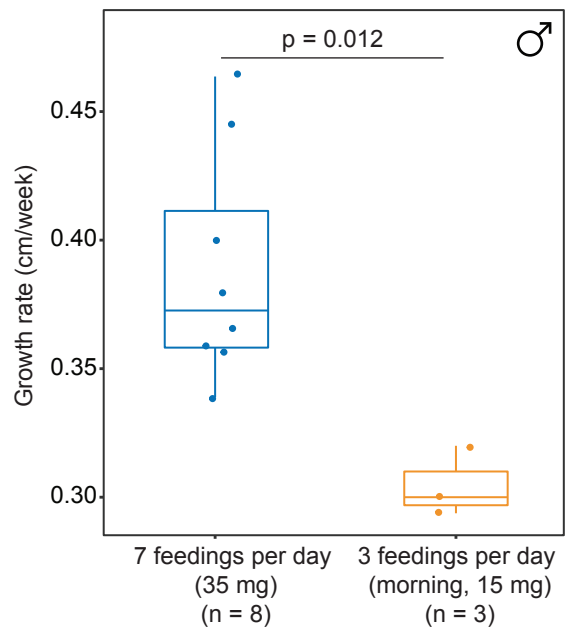

C Female growth rate upon dietary restriction

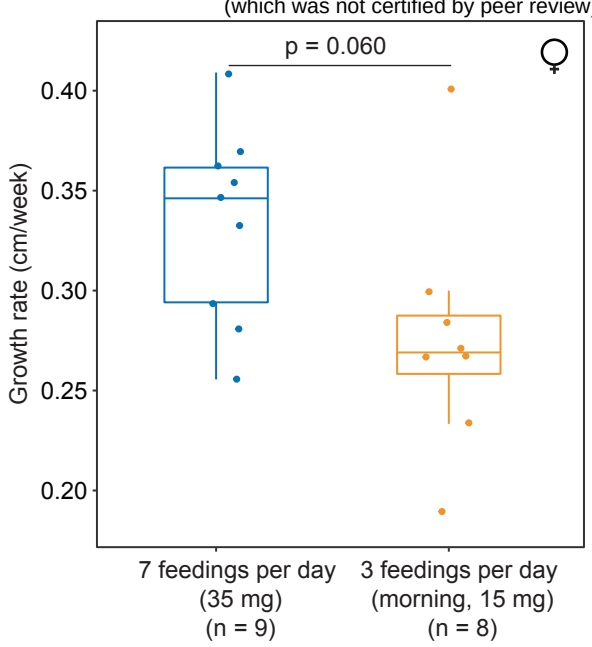

D Fertilized embryos produced upon dietary restriction

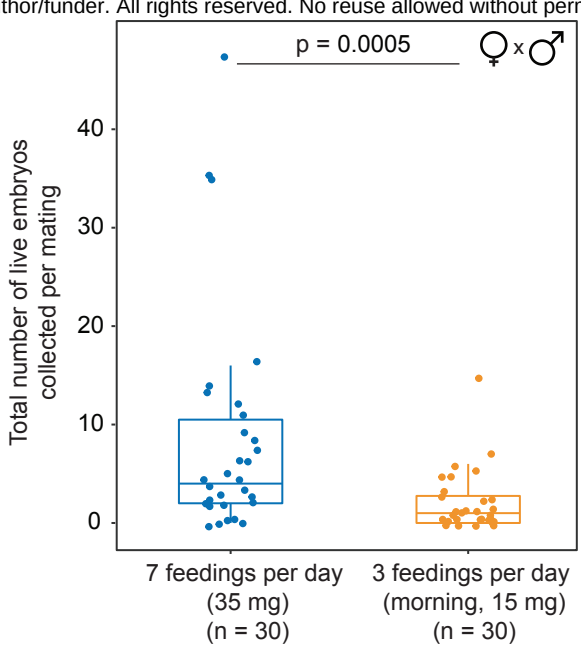

E Experimental scheme for overfeeding

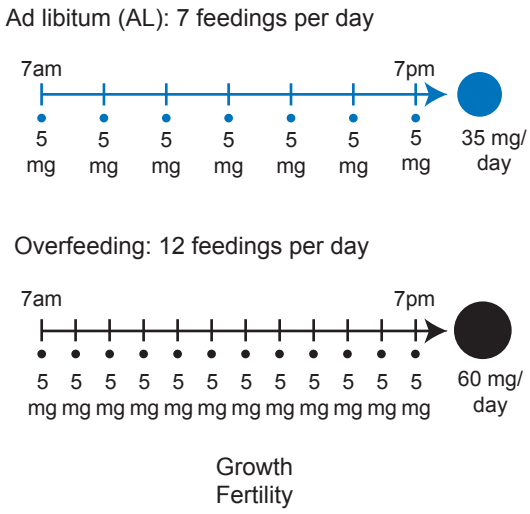

F Male growth rate upon overfeeding

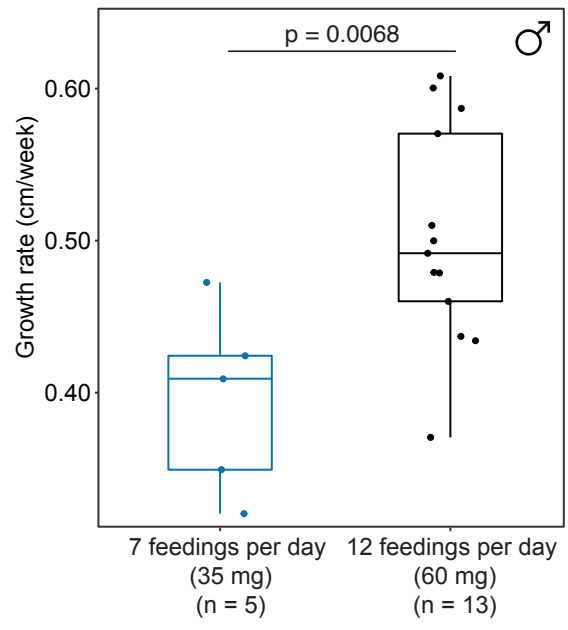

G Female growth rate upon overfeeding

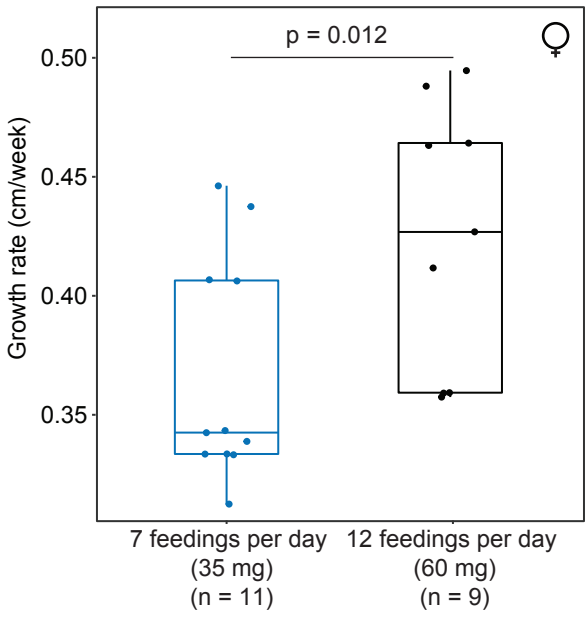

H Fertilized embryos produced upon overfeeding

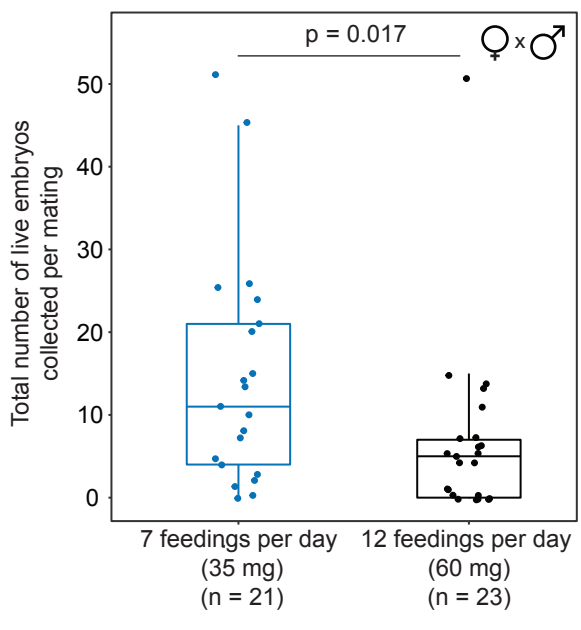

Figure 4

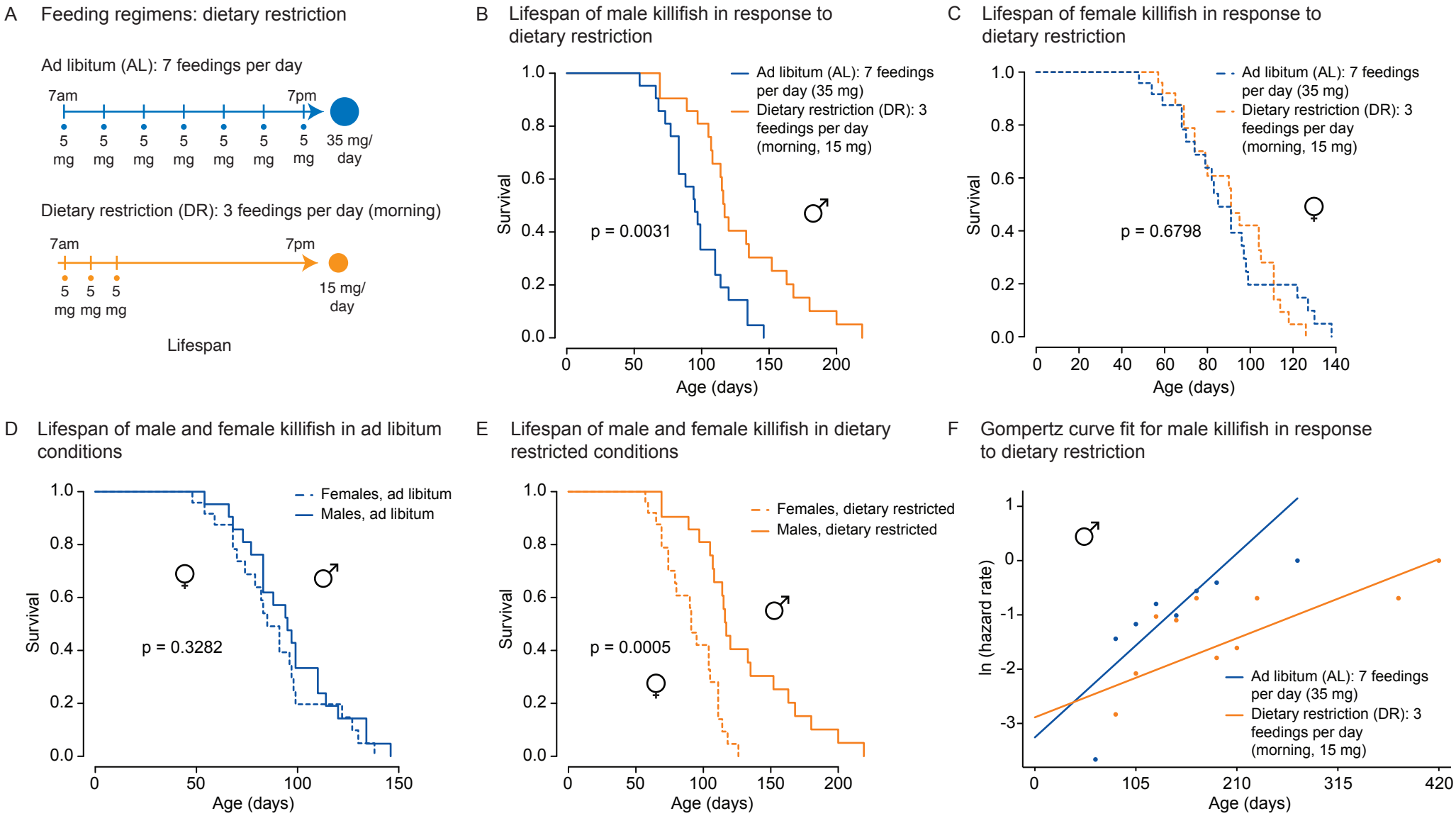
A
Feeding regimens: dietary restriction
Ad libitum (AL): 7 feedings per day
7am
7pm
5 mg
5 mg
5 mg
5 mg
5 mg
5 mg
5 mg
35 mg/ day
Dietary restriction (DR): 3 feedings per day (morning)
7am
7pm
5 mg
5 mg
5 mg
15 mg/ day
Lifespan
B
Lifespan of male killifish in response to dietary restriction
Survival
Age (days)
Ad libitum (AL): 7 feedings per day (35 mg)
Dietary restriction (DR): 3 feedings per day (morning, 15 mg)
p = 0.0031
C
Lifespan of female killifish in response to dietary restriction
Survival
Age (days)
Ad libitum (AL): 7 feedings per day (35 mg)
Dietary restriction (DR): 3 feedings per day (morning, 15 mg)
p = 0.6798
D
Lifespan of male and female killifish in ad libitum conditions
Survival
Age (days)
Females, ad libitum
Males, ad libitum
p = 0.3282
E
Lifespan of male and female killifish in dietary restricted conditions
Survival
Age (days)
Females, dietary restricted
Males, dietary restricted
p = 0.0005
F
Gompertz curve fit for male killifish in response to dietary restriction
ln (hazard rate)
Age (days)
Ad libitum (AL): 7 feedings per day (35 mg)
Dietary restriction (DR): 3 feedings per day (morning, 15 mg)

Figure 5

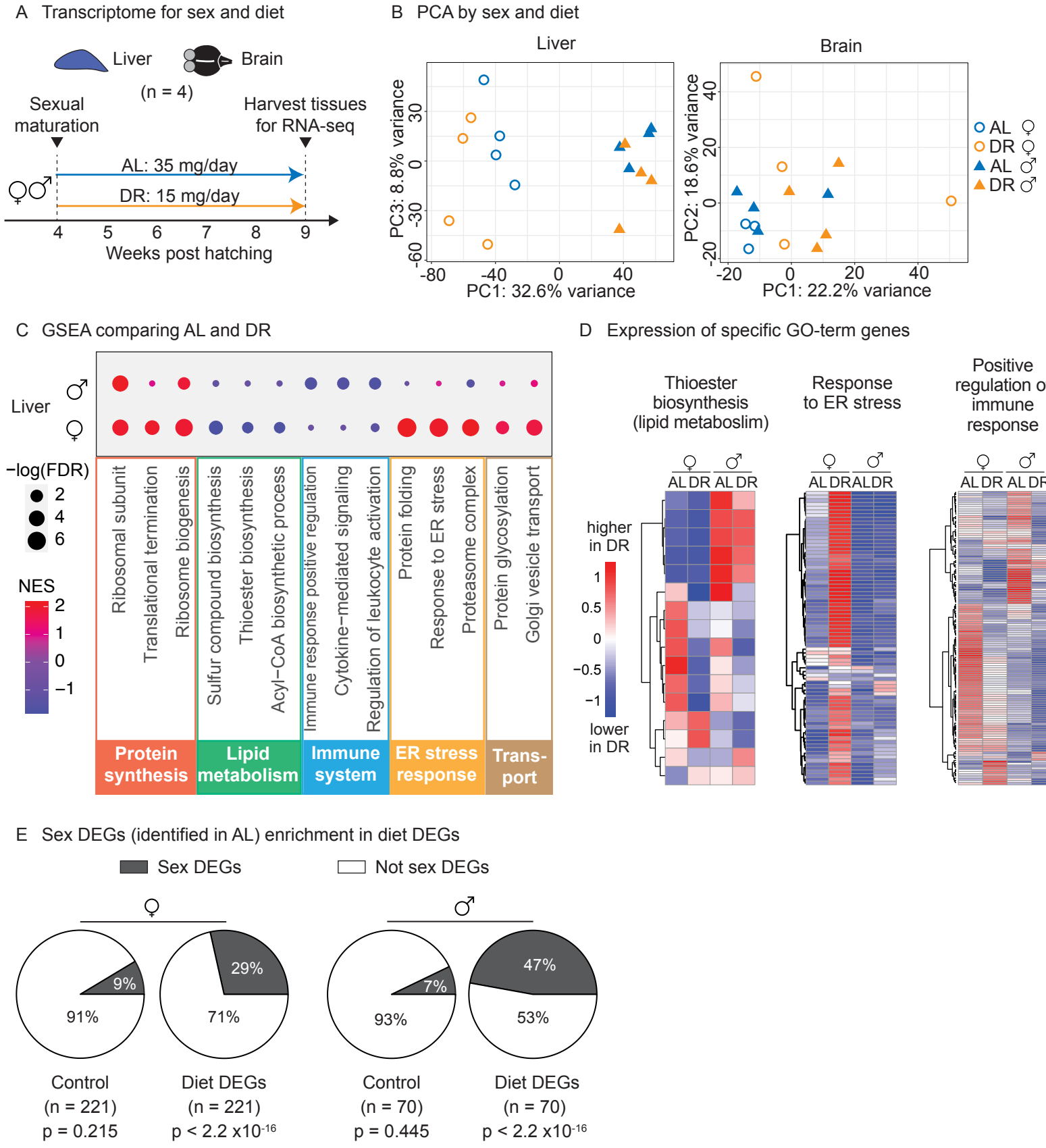

Figure 6

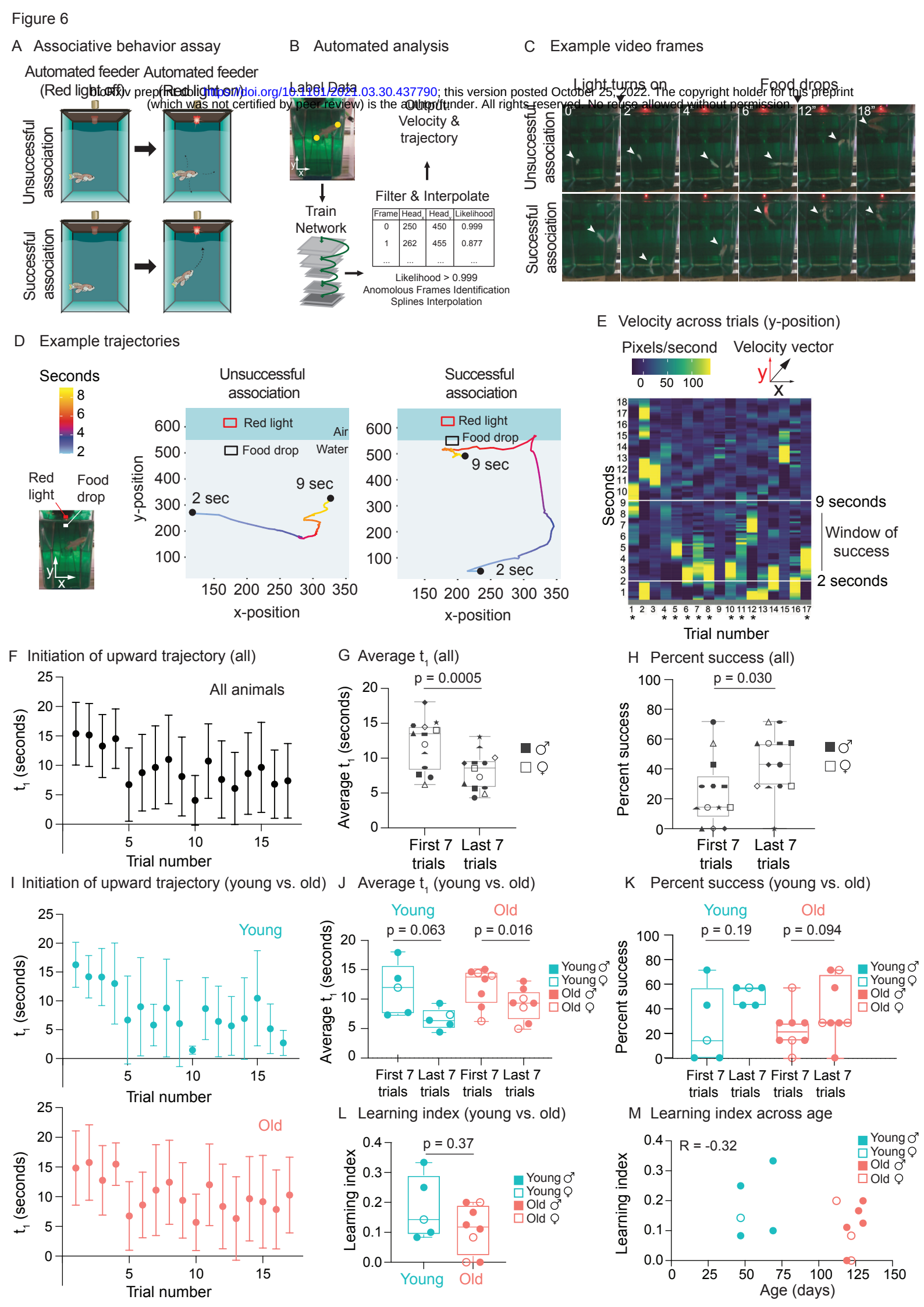

Figure 1- figure supplement 1

A Schematic for feeder operation

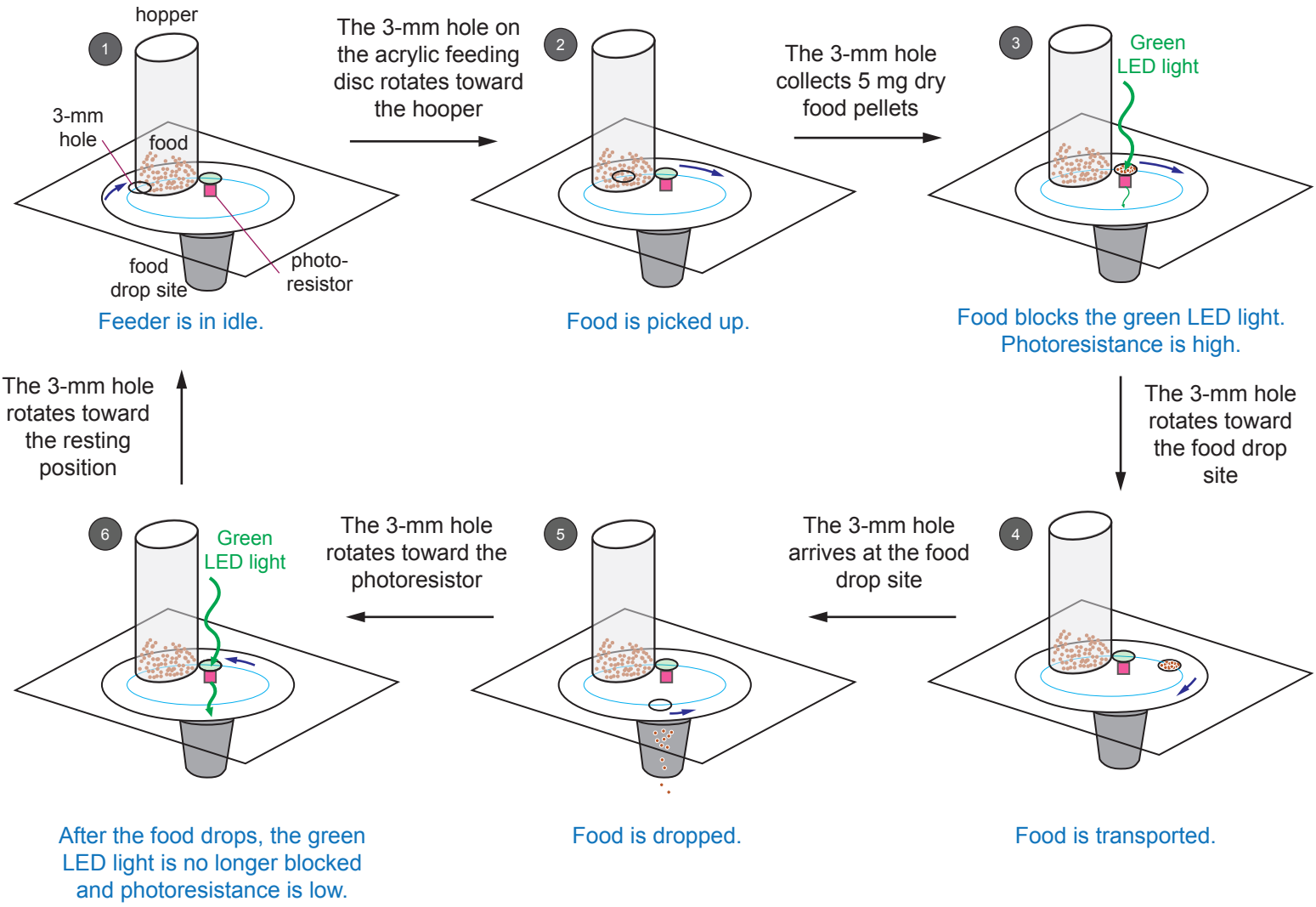

B Schematic for the independence of each feeder's feeding regimen

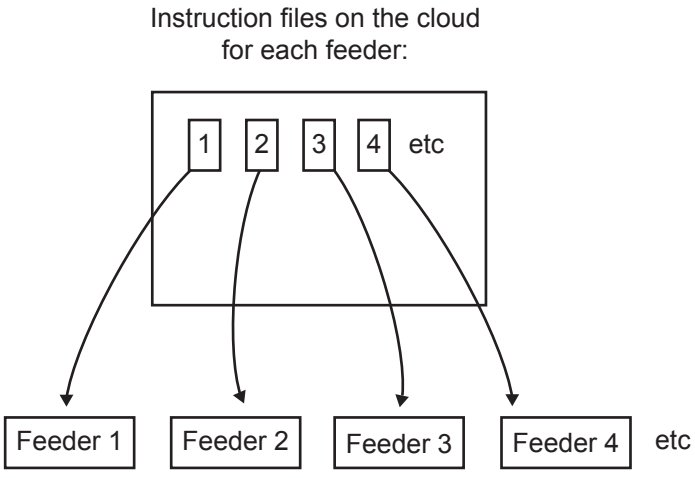

Figure 2 - figure supplement 1

A Fidelity of multiple automated feeders

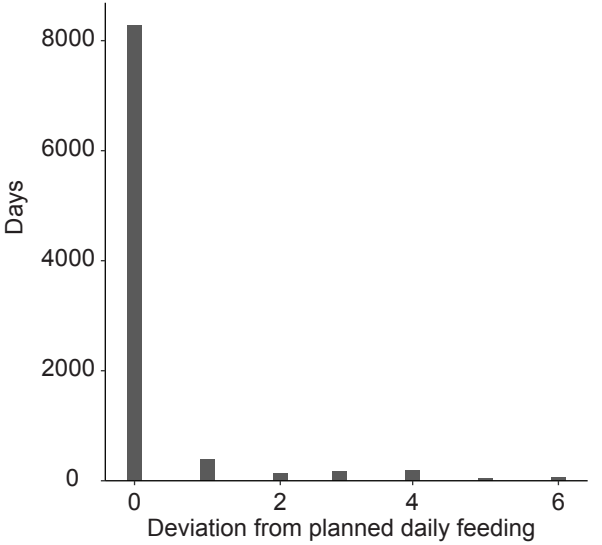

B Feeding number and frequency

Deviation from planned daily feeding	Days	Frequency
0	8275	89.13%
1	388	4.18%
2	130	1.40%
3	180	1.94%
4	197	2.12%
5	53	0.57%
6	61	0.66%

Figure 3 - figure supplement 1

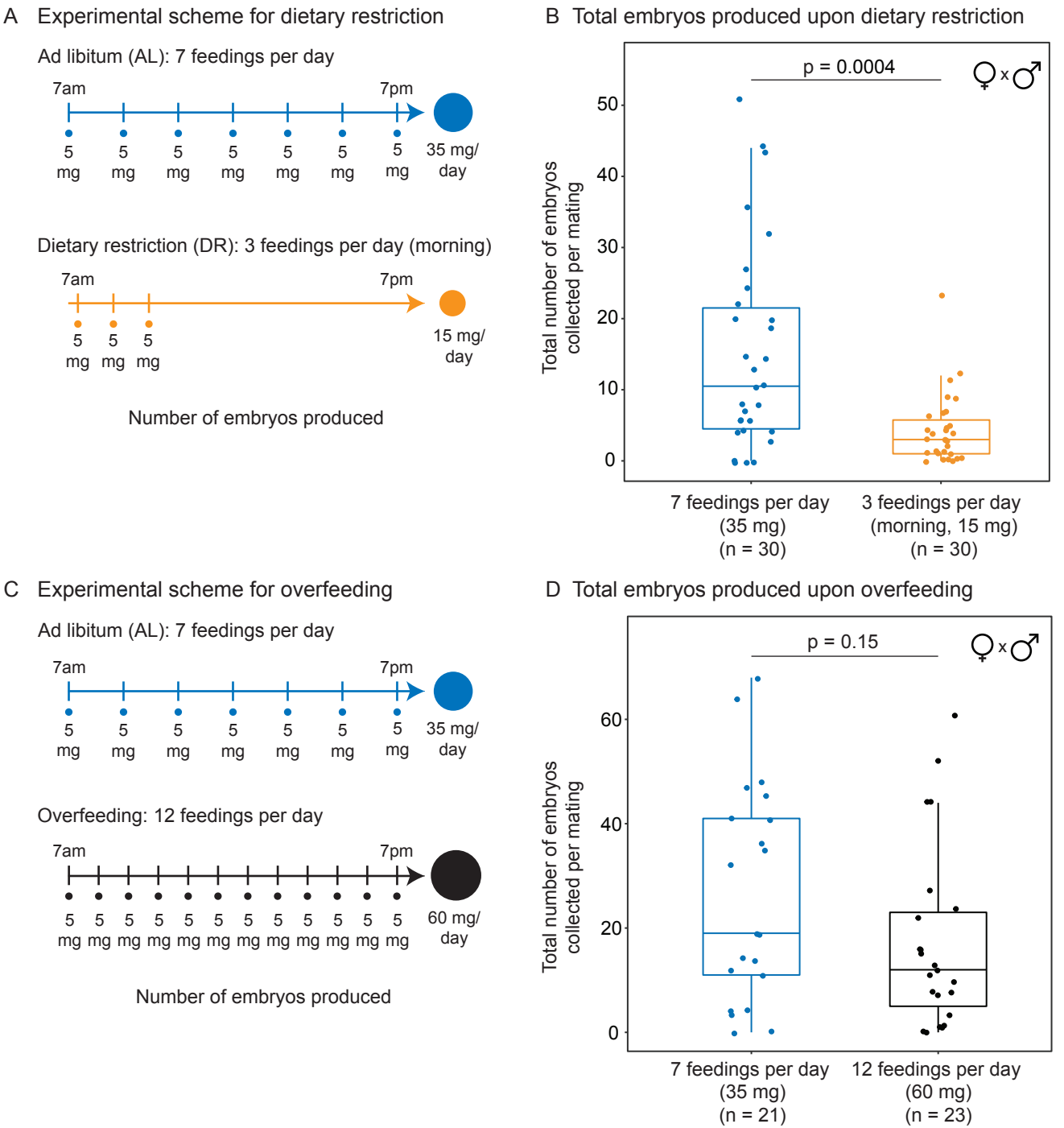

Figure 4 - figure supplement 1

A Feeding regimens: dietary restriction

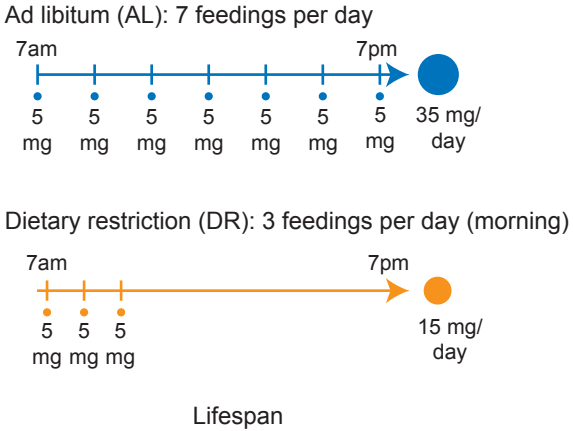

B Lifespan of male killifish in response to dietary restriction (cohort 1)

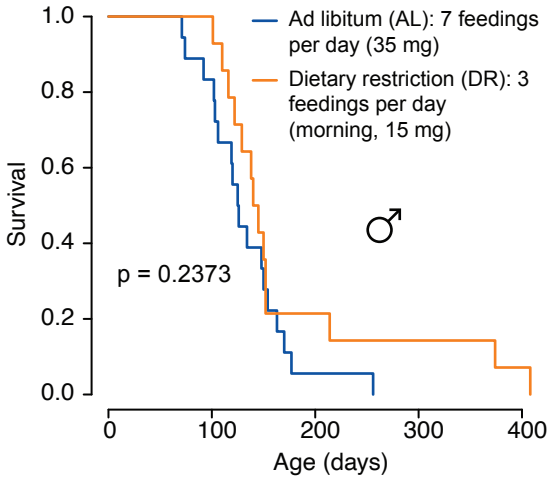

C Lifespan of female killifish in response to dietary restriction (cohort 1)

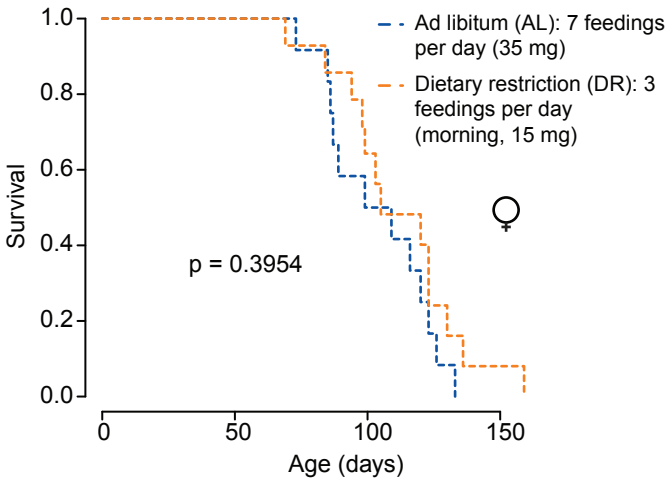

D Lifespan of male and female killifish in ad libitum conditions (cohort 1)

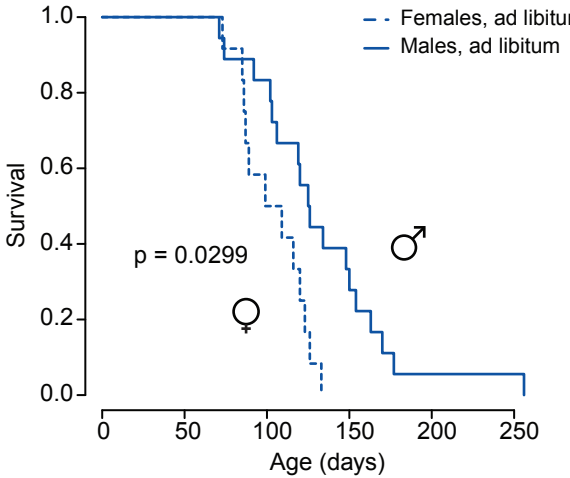

E Lifespan of male and female killifish in dietary restricted conditions (cohort 1)

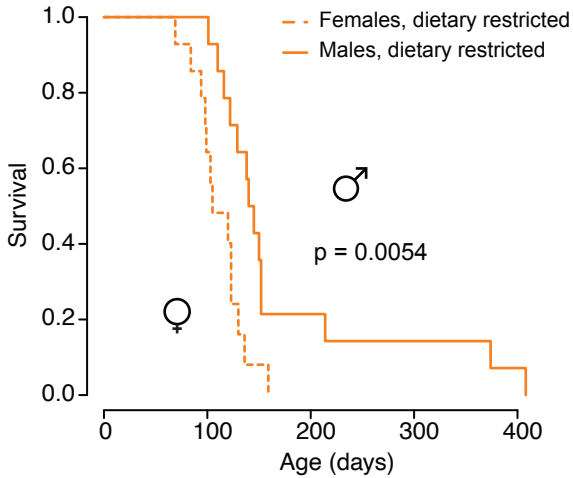

F Combined lifespan for both cohorts of male killifish in ad libitum or dietary restriction conditions

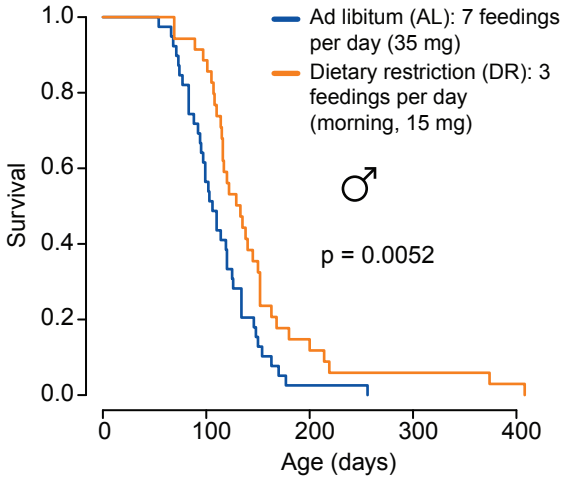

Figure 5 - figure supplement 1

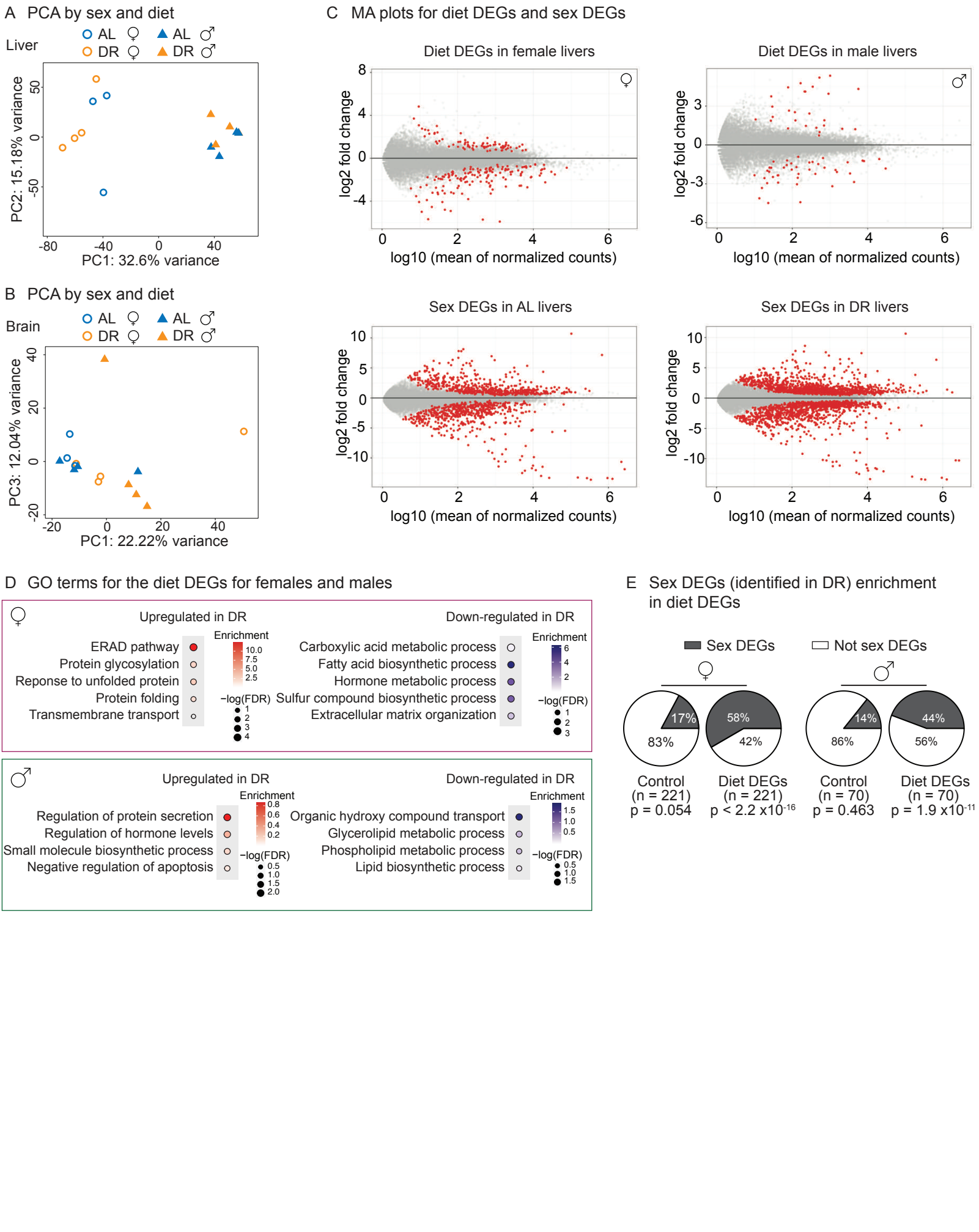

Figure 6 - figure supplement 1

A Compass plots

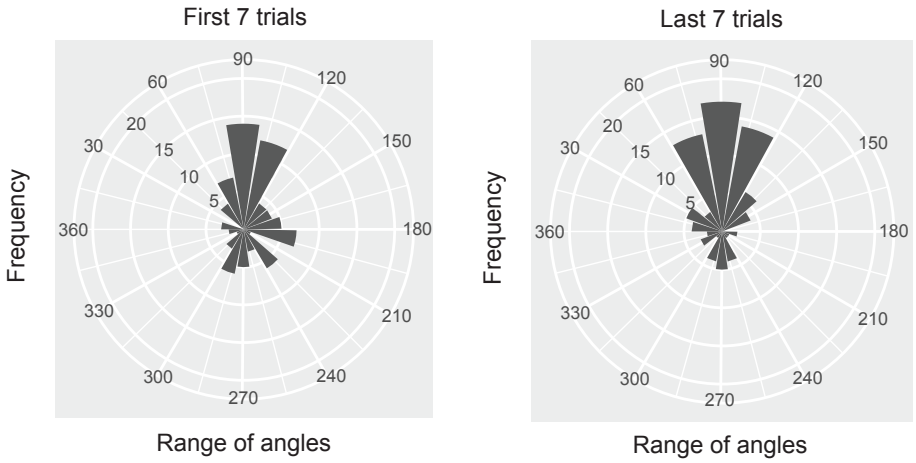

B Manual quantification pipeline and example record

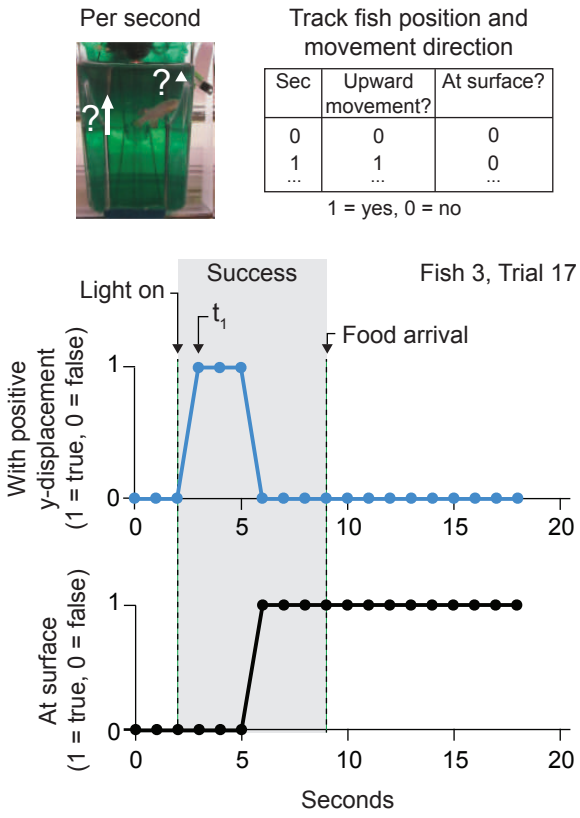

D Average t_1 (all)

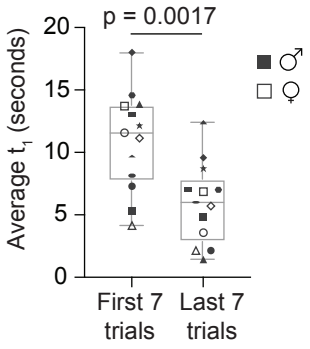

E Percent success (all)

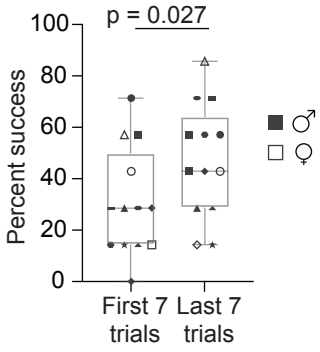

F Correlation of automated and manual analysis

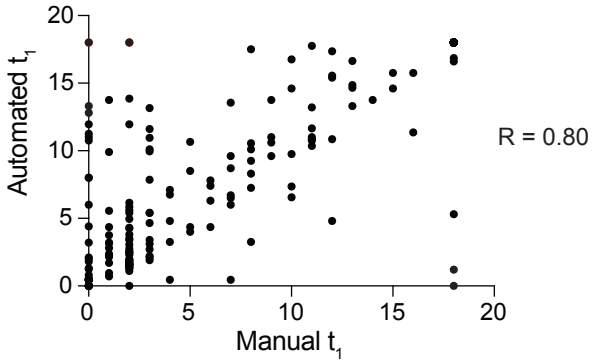

C Initiation of upward trajectory (all)

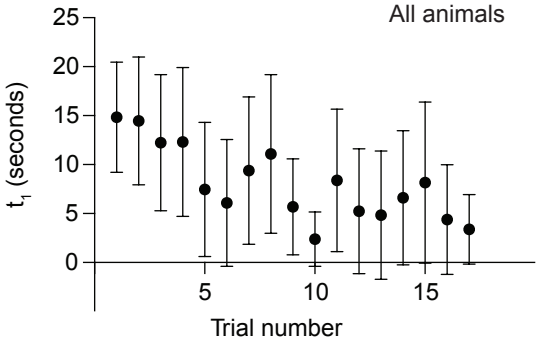

G Average velocity (young vs. old)